INCOMPATIBLITY-GOVERNED DEFORMATIONS: TOWARDS A NEW MODEL OF SMALL-STRAIN ELASTOPLASTICITY

Samuel Amstutz, Thien-Nga Le, Nicolas van Goethem

INCOMPATIBLITY-GOVERNED DEFORMATIONS: TOWARDS A NEW MODEL OF SMALL-STRAIN ELASTOPLASTICITY

SAMUEL AMSTUTZ, THIÊN-NGA LÊ, AND NICOLAS VAN GOETHEM

Abstract. We describe a novel formalism for elasto-plastic deformations based on the strain incompatibility, to model an elastic solid filled with dislocations, hence subject to plastic deformations, at the macroscopic scale and under a time-discrete quasi-static framework. The main kinematical descriptor is the strain tensor E, that we define from a mesoscopic analysis. The associated state equations, as derived from a virtual work approach, are second-gradient in E, because they explicitly incorporate the incompatibility $\operatorname{inc} E$, and are linear. Due to the introduction of an internal variable θ and a dissipation potential, related to the motion of dislocations, the overall problem is variational and nonlinear. It is numerically solved by alternating minimization with respect to (E, θ). Numerical simulations are performed to assess both loading-unloading and evolutionary problems on some simple two-dimensional geometries. Elaborating on previous works by the authors, the present contribution is an in-depth description of an alternative approach to elasto-plastic deformations, grounded on firm mathematical basis, and consolidated by numerical results. By nature, this approach is multi-scale, therefore opening the way to a comprehensive study of strain incompatibility, dislocations and plasticity as a complex interaction of multiscale phenomena, of which hardening is only an archetypal example.

1. Introduction

The theory of small-strain elasto-plasticity has experienced significant developments during the second part of the twentieth century, partly thanks to the fruitful interaction between mathematics and mechanics. As a consequence, models have emerged, typically based on convex analysis, and have proved successful. Some of them are time-continuous, others incremental, or variational. In the former case they are inherently rate-dependent: the evolution of plastic strain explicitly depends on the rate of loading or stress. The majority of these models are designed in the framework of Continuum mechanics at the macroscopic scale; they model the elasto-plastic deformation using the traditional decomposition of the strain in elastic and plastic parts. Typically, the system of equations is the balance of momentum, coupled with some ad-hoc *flow rules* to describe the plastic flow. In incremental formulations, the unknowns at the end of the increment are obtained by solving a time-independent problem. In the primal variational formulation [23], a dissipation function is introduced to pose the associated variational problem. We refer to Simo & Hugues and Han & Reddy classical textbooks [23, 36] for an introduction to these models (see also the comprehensive reference [21]). Plastic flow occurs due to the motion of dislocations at a lower scale, but it is rare to find a macroscopic model taking into account the time-evolution of the density of dislocations, a tensorial quantity, besides the classical kinematical fields. Alternatively, the flow law in crystals can be described at a finer level, the mesoscopic scale, introducing explicitely glide planes, dislocation line orientation and Burgers vectors. Such models, explored by Mura [33] or described in Acharya's seminal papers [2], and further developed in a number of papers [1,14,17,18,20,24,29,30,37], assume constitutive equations for dislocation glide, and derive evolution equations for the deformation tensors and the dislocation density (notably in the references [2,4]), even in the finite-strain context. They also use the traditional decomposition between elastic and plastic strain.

In our model, we depart from the classical approach from the start, by choosing novel model variables. We describe a formalism based on the concept of strain incompatibility, specifically,

Key words and phrases. Elasticity, plasticity, strain incompatibility, dislocations, virtual work, dissipation.

we introduce a (non-conventional) strain field E, together with its incompatibility $\operatorname{inc} E := \operatorname{Curl}(\operatorname{Curl} E)^T$, that are used to model a deformable solid filled with dislocations, hence subject to plastic deformations, at the macroscopic scale and under a time-discrete, quasi-static, rate-independent framework. One of our goals in defining this new kinematical descriptor E is to depart from the traditional decomposition $\epsilon = \epsilon^e + \epsilon^p$ of the total, compatible, small-strain field which stems from the linearization of decomposition $F = F^e F^p$ of the deformation gradient. This multiplicative decomposition raises known intermediate configuration issues, notably due to its non-smoothness and arbitrary character, therefore leading to a lack of theoretical consistency [45]. Crucial in our model is the fact that the second-order symmetric tensor E needs not be a symmetric gradient.

We typically consider single crystals. Our model is isotropic, though it could in principle take into account anisotropy, by taking appropriate tensor constitutive laws. Our equilibrium equations, derived from a classical virtual work approach, involve two kinds of internal efforts, working against E and $\operatorname{inc} E$, respectively. Our framework enables the computation of E at each time step by solving a combination of an equilibrium equation and a flow rule, in a coupled form. The former involves effective elasto-plastic moduli derived from the latter, which itself relies on thermodynamic arguments. The model is thus overall nonlinear, due to the treatment of dissipation, incremental, and belongs to the family of higher-gradient models.

We emphasize that our model is not grounded on mesoscopic dislocation movements, however dislocations may be present at any location and with any orientation, because strain incompatibility is related to dislocation density. Indeed, ultimately, by the celebrated Kröner's formula we make the link between strain incompatibility and local variations of dislocation density. Thus, in this model, motion, annihilation or nucleation of dislocations are neither taken into account nor excluded: the model simply considers stock of the incompatibility between two instants.

To comply with the second Principle, we need to tackle the modelling of dissipation as well. The flow rule is inferred from the Clausius-Duhem inequality, in which the dissipative effects are controlled by a dissipation potential, and via the introduction of an internal variable, called *compatibility modulus* related to the underlying dislocation microstructure. With these ingredients, we construct the incremental scheme in which the evolution over one time step is given by solving a double minimization problem. With relatively simple numerical techniques, we are able to perform some illustrative numerical simulations for academic problems. Note also that the combination of different orders of spatial derivatives within the model allows one, in principle, to address size-scaling issues [43].

Our model eventually writes as a double minimization problem. The overall approach is close in spirit to crack evolution descriptions based on optimization methods [5,44], and is the continuation of the works on the subject by the first and last authors. In particular, preliminary versions of the model, as well as their mathematical foundation, have been published in a series of papers [9–11], as an extension and elaboration of the *distributional approach* [39, 40]. In particular, we refer here indeed to some of the authors' earlier work (see [8, 11] and references therein) which gives the in-depth mathematical proofs needed to ensure the validity of the variational equations in the relevant spaces for our problem. As compared to our last paper [8], this one gives therefore deeper insight into the mesoscopic nature of our kinematic fields, and introduces a methodology to include hardening in an incremental framework, giving rise to numerical simulations on some simple geometries. In particular loading-unloading examples and incremental plasticity are assessed.

Despite the eventual macroscopic character of the model, we believe important and illuminating to justify its construction by exploring its origin at a mesoscopic scale in a rigorous manner, in particular for the construction of the main kinematical variable E, and for the interpretation of the concept of incompatibility in our framework. This enables us to compare our novel fields with the classical ones, and to show, incidentally, that our kinematical variable $\operatorname{inc} E$ corresponds to Kröner's classical "measure of incompatibility" $\eta = \operatorname{inc} \epsilon^e$, which has a simple interpretation in terms of the dislocation density tensor in single crystals [25, 38].

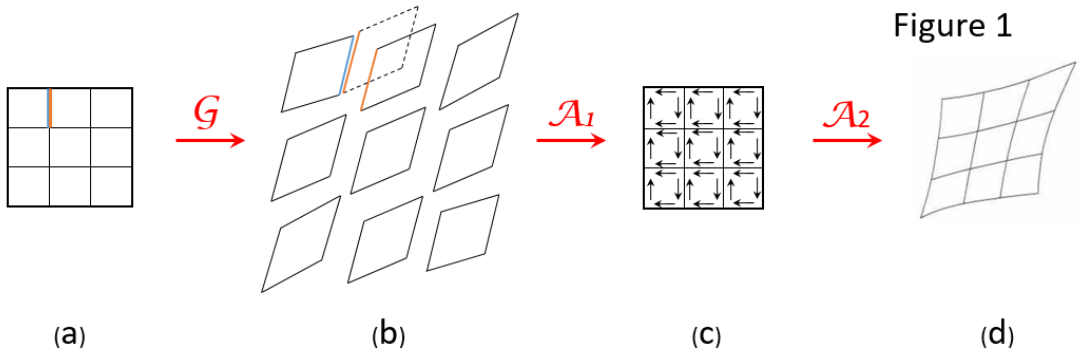

FIGURE 1. (a) an initially cohesive 2D square in split in equal-sized squares; (b) each of the squares is homogeneously deformed, note that the deformation is not the same for all squares. Area has been kept constant. The dotted parallelogram has been translated to show the mismatch between the orange and blue borders, a sign of incompatibility. To evidence this fact this figure is enlarged compared to the others; (c) some efforts are introduced to make the assembly compact again; (d) the total square is relaxed elastically. (Adapted from Kröner).

Our paper will be structured as follows: Section 2 deals with aspects of incompatibility, namely the decomposition in elastic and plastic parts, the question of the intermediate configuration, and recalls the interpretation of classical incompatibility in terms of the Nye tensor [27]. In Section 3 our reworking of usual quantities is explained, at the mesoscopic scale, in particular with the new definition of the strain E. In Section 4, we illustrate the theory on a simple example of Volterra dislocation. Section 5 allows us to define the fields at the macroscopic scale, and Section 6 encloses formulations at the macroscale, for the virtual work principle, the tangent moduli, and introduces constitutive laws. In Section 7, the second principle of thermodynamics, dissipation and flow rules are discussed, by means of the introduction of an internal variable; in particular, the connection with classical Hencky plasticity is made. Section 8 addresses the time-discrete variational formulation, and the simple but illuminating loading-unloading test, while Section 9 discusses the introduction of hardening in the model, allowing for the computation of incremental plasticity. In Section 10 we finally give a numerical method to solve the double minimization, as well as a couple of simple examples in 2D. Further computations require involved numerics, and will be the object of future work.

2. INCOMPATIBILITY FOR FINITE AND INFINITESIMAL DEFORMATIONS

2.1. **Finite deformation context - the intermediate configuration problem.** In order to first clarify the concept of incompatibility in the finite-deformation context, we refer to Fig. 1, adapted from Kröner [27]. A square body is submitted to a deformation gradient $\mathcal{F}$. The Kröner (or Kröner-Lee) decomposition is a multiplicative decomposition written as $\mathcal{F} = F^e F^p$, where F^p and F^e are the plastic and elastic distortion tensor fields, respectively. The term distortion, see e.g. [21], describes the transformation of infinitesimal fibers. It may be a deformation gradient, or not. In order to describe F^e and F^p in a heuristic way, the transformation is decomposed into a sequence of steps. The Gedanken experiment is the following: firstly, the body is split in smaller squares; tote that the size of the squares is arbitrary (Fig. 1(a)).

The first step is described by the distortion $\mathcal{G}$, of which a schematic representation by the deformed squares is given in Fig. 1(b). Each square is deformed independently, and it can be seen that the blue and orange borders of the corner square do not match with each other. This misalignment prevents $\mathcal{G}$ from being a deformation gradient: it is said to be incompatible. The tensor $\mathcal{G}$ represents the result of a succession of slips occuring at a smaller scale, enabled by the motion of dislocations. However, according to [21], "slips (as fields on the individual slip systems) are not well-defined quantities: what are well defined are slip rates": we will elaborate on that point later. We call $\mathcal{G}$ the plastic distortion and set $F^p = \mathcal{G}$.

On Fig. 1(c) is depicted the reverse deformation consisting in gluing back all pieces together in order to recover the body on Fig. 1(a). However it is important to notice that, although kinematically the pieces are deformed by $\mathcal{A}_1 = \mathcal{G}^{-1}$, some efforts have been applied to the faces to make them match again.

Finally these efforts are released, and the resulting distortion $\mathcal{A}_2$ yields the body on Fig. 1(d). This latter step results in a compatible deformation from Fig. 1(a) to Fig. 1(d), as shown by the absence of discontinuities in the final deformed body. So, in the general finite deformation classical context of elastoplasticity we have:

$$\mathcal{F} = \mathcal{A}_2 = \mathcal{A}_2(\mathcal{A}_1\mathcal{G}) = (\mathcal{A}_2\mathcal{A}_1)\mathcal{G} = F^e F^p.$$

The distortion $F^e := \mathcal{A}_2\mathcal{A}_1$ is identified as elastic because it is associated with internal efforts, in contrast to the plastic part F^p, which is sometimes for this reason connected to the concept of *eigenstrain*. Although $\mathcal{F}$ is by construction the gradient of a smooth function, F^e and F^p are not. In other terms, there exists no well-defined intermediate configuration associated with the distortion F^p. Indeed, the authors in [19] showed that an intermediate configuration with metric $(F^p)^T F^p$ can be found as a Riemannian manifold embedded in a higher dimensional space, sometimes even with uniqueness, but not as a subspace of the ambient space.

2.2. **Infinitesimal context.** When F^p and F^e are small perturbations of the identity we write (for some globally-defined displacement field u, though itself not necessarily small) $\mathcal{F} = \mathrm{Id} + \beta = \mathrm{Id} + \nabla u$, $F^{p,e} = \mathrm{Id} + \beta^{p,e}$, and we get at the first order:

$$\nabla u = \beta = \beta^p + \beta^e. \tag{2.1}$$

While in this setting compatibility is characterized by $\operatorname{Curl} \beta = 0$, the plastic and elastic infinitesimal distortion fields β^p and β^e are possibly incompatible, i.e. $\operatorname{Curl} \beta^{p,e}$ do not vanish in general.

At the meso-scale where kinematic singularities are allowed, we can interpret (2.1) as the Radon-Nikodým decomposition [7] of the distributional gradient ∇u. Specifically, β^p is a concentrated measure which accounts for slips, i.e. $\beta^p = \mathcal{S}\delta_\Gamma$ where Γ is the slip surface, δ_Γ is the surface Dirac measure, $\mathcal{S}$ is the Schmid tensor, while β^e is the absolutely continuous (or diffuse) part. When Γ is planar, this is the Volterra dislocation model. Its equivalence to conventional plasticity is discussed in [3], introducing thickened slip regions and dislocation cores of finite size to prevent the unboundedness of the elastic energy. The Radon-Nikodým decomposition, when applied to the symmetric gradient, will be essential for building our own model. It will be developed in detail in Section 3.1.

In the celebrated work to which we referred [25], Kröner further identifies

$$\alpha := \operatorname{Curl} \beta^p = -\operatorname{Curl} \beta^e$$

as the tensor of dislocation density, or Nye's tensor, and derives the second order incompatibility equations $\operatorname{inc} \epsilon^e = -\operatorname{Curl} \kappa = \eta$, where κ is the *contortion tensor* (called *Cosserat-Nye tensor* by Kröner [26]),

$$\kappa =: \alpha^T - \frac{1}{2}\operatorname{tr}(\alpha)\,\mathrm{Id}.$$

In practice, tensor α gives the Burgers vector db_i of a dislocation that crosses a surface element dS_j (that is, $db_i = \alpha_{ij} dS_j$), whereas the Cosserat-Nye tensor κ represents the relative rotation of the lattice structure at two points that lie dx_i apart (that is, $d\theta_i = \kappa_{ij} dx_j$) [26].

Let us now prove Kröner's formula

$$\text{inc } \epsilon^e = -\,\text{Curl } \kappa,$$

assuming that the fields and the derivative operator are intended in the distribution sense. Here, the tensorial curl is defined row-wise, i.e. $(\text{Curl } E)_{ij} = \varepsilon_{jkl}\partial_k E_{il}$. We decompose β^e into its symmetric and skewsymmetric parts, $\epsilon^e := \frac{1}{2}\left(\beta^e + (\beta^e)^T\right)$ and $\omega^e := \frac{1}{2}\left(\beta^e - (\beta^e)^T\right)$, so that

$$\beta^e = \epsilon^e + \omega^e.$$

The quantity $\text{inc } \epsilon^e := \text{Curl } (\text{Curl } \epsilon^e)^T$ is a measure of incompatibility since it vanishes over a simply connected domain if and only if ϵ^e is a symmetric gradient. We notice that $\omega^e_{il} = \varepsilon_{ilm}\omega_m$ with $\omega_i := \frac{1}{2}\varepsilon_{ikl}\beta^e_{kl}$. Further, $\text{div } \omega = \partial_i \omega_i = -\frac{1}{2}\,\text{tr Curl } \beta^e = \frac{1}{2}\,\text{tr}\,\alpha$. Now,

$$\text{Curl } \epsilon^e = \text{Curl } \beta^e - \text{Curl } \omega^e = \text{Curl } \beta^e - \nabla^T\omega + (\text{div } \omega)\text{Id},$$

and hence

$$\text{inc } \epsilon^e := \text{Curl } (\text{Curl } \epsilon^e)^T = \text{Curl } \left(\text{Curl } \beta^e - \nabla^T\omega + (\text{div } \omega)\text{Id}\right)^T = -\,\text{Curl } \left(\alpha^T - \frac{1}{2}\,\text{tr}\,\alpha\,\text{Id}\right).$$

3. Kinematics at the mesoscopic scale: Radon-Nikodým encounters Beltrami

The mesoscopic scale is a scale at which some kinematical singularities are allowed. More precisely, in the infinitesimal deformation framework in which we place ourselves,

- dislocations are represented by field singularities, i.e., some fields (distortion, strain or components thereof) become unbounded as one approaches the dislocation; here the dislocation is typically modeled by a line;
- slips are modeled by means of concentrated fields on some lower-dimensional subsets, typically slip (or glide) planes in 3d, actually half planes bounded by the dislocation line.

3.1. The Radon-Nikodým decomposition of the compatible strain.

Our starting point is a displacement field u, which is typically assumed to be locally integrable, i.e., $u \in L^1_{\text{loc}}(\Omega;\mathbb{R}^3)$. Its symmetric gradient $\nabla^S u$ is a tensor-valued distribution. In the presence of a glide surface Γ, u admits a jump $[\![u]\!]$. Our convention with jumps is to count positively the contribution with N outwards, where N is a chosen unit normal to Γ. Under mild assumptions, namely that $u \in SBD_{\text{loc}}(\Omega)$, the Radon-Nikodým decomposition [6, 7] of the symmetric gradient reads

$$\epsilon := \nabla^S u = \bar{\nabla}^S u - [\![u]\!] \odot N\delta_\Gamma, \tag{3.1}$$

with $\odot$ the symmetric tensor product. The absolutely continuous part $\bar{\nabla}^S u$ is non-concentrated, in mathematical terms it belongs to the space of (locally) Lebesgue-integrable functions $L^1_{\text{loc}}(\Omega;\mathbb{S}^3)$. Note that it is a symmetric tensor yet not a symmetric gradient, therefore the symbol $\bar{\nabla}$ is not strictly speaking a gradient; however $\bar{\nabla}^S u$ is almost everywhere a symmetric gradient [6]. The displacement jumps on Γ result in the contribution $[\![u]\!]\odot N\delta_\Gamma$, with δ_Γ standing for the concentrated Hausdorff measure on Γ, a particular surface Dirac delta.

In order to retrieve the conventional view of infinitesimal plasticity, one is tempted to identify $\bar{\nabla}^S u$ with the elastic strain $\epsilon^e := (\beta^e + (\beta^e)^T)/2$, and to interpret the concentrated part $-[\![u]\!]\odot N\delta_\Gamma$ as the plastic strain $\epsilon^p := (\beta^p + (\beta^p)^T)/2$. Then we recover the classical additive decomposition $\epsilon = \epsilon^e + \epsilon^p$ at the mesoscale already discussed in Section 2.2.

Nevertheless it is important to note that whenever the jump $[\![u]\!]$ is assumed constant on a surface Γ with a boundary, which is the case in the Volterra construction of a mesoscopic dislocation, it can be proved [34, 35] that $\bar{\nabla}^S u$ cannot be square-integrable. In fact it is only in $L^p_{\text{loc}}(\Omega;\mathbb{S}^3)$ with $1 \le p < 2$. Even when the jump varies gradually over a small region (dislocation core), $\|\bar{\nabla}^S u\|_{L^2}$ is finite but large. We believe this to be problematic for a model with a quadratic stored-elastic energy fully involving $\bar{\nabla}^S u$. Another related aspect is that the displacement jump yields matter

"self-penetration" at the dislocation line, where a singularity is provoked by the constant jump on the half plane. This is acceptable since atomic disturbances occur in this region, but reveals the lack of physical meaning of $\bar{\nabla}^S u$ there. In order to intuitively appraise how concentrated incompatibility yields strain singularity, let us rather consider a non-constant jump, with tangential components varying from 0 to b over a small distance h to the dislocation, as shown by two of the authors in [8]. Then $\bar{\nabla}^S u$ admits components of order b/h, which obviously blows up when h goes to 0. This argument is also raised in [3], where it is circumvented with the help of a finite dislocation core. A variable jump nearby the singularity is also discussed in [16], where an asymptotic analysis is made.

In our model we consider as main kinematical descriptor the (total) strain defined by means of a small correction ϵ', that is

$$E := \epsilon - \epsilon' = (\epsilon^e - \epsilon') + \epsilon^p, \tag{3.2}$$

in such a way that $\bar{E} := \epsilon^e - \epsilon'$ is at the same time

- compatible
- diffuse
- the correction ϵ' is as small as possible.

We will later explain and mathematically specify these choices. Remember that ϵ^p is

- incompatible
- concentrated
- related to a physical glide plane, in particular it is reasonable to assume[1] that $\operatorname{tr} \epsilon^p = 0$.

By this construction, E is the sum of a regular part and a trace-free part, something natural in plastic flows, since no volume changes are expected. This latter one being concentrated, it may be large even in a macroscopic setting, and this will be handled by tuning the shear modulus to control the stress.

Thus the strain incompatibility is, up to a sign, the Kröner-Nye's incompatibility tensor,

$$\operatorname{inc}\ E = \operatorname{inc}\ \epsilon^p = -\operatorname{inc}\ \epsilon^e = -\eta = \operatorname{Curl} \kappa. \tag{3.3}$$

The mechanical phenomena occurring within dislocation cores will be taken into account through $\operatorname{inc} E$, rather than E itself. The following subsection shows the mathematical construction leading to the precise definition of E.

3.2. **Beltrami decomposition.** The mathematical decomposition property called Beltrami decomposition of a generic symmetric tensor field $\mathbb{E}$ with values in $L^p_{\mathrm{loc}}(\Omega;\mathbb{S}^3)$ with $1 \le p < 2$ has been proved in [31] and refined in [9,11]. It consists in writing

$$\mathbb{E} = \nabla^S v + \mathbb{E}^i,$$

where $\mathbb{E}^i$ is a *divergence-free* symmetric tensor, called the incompatible part of $\mathbb{E}$, whereas $\nabla^S v$ is the compatible part, written in terms of a displacement field v. The uniqueness of v and $\mathbb{E}^i$ is ensured by appropriate boundary conditions, in which case the decomposition is L^2-orthogonal [11,31]. For the sake of conciseness and clarity we omit boundary conditions.

Applying this decomposition to the symmetric tensor $\mathbb{E} = \bar{\nabla}^S u$ yields

$$\bar{\nabla}^S u = \nabla^S \bar{u} + F, \tag{3.4}$$

where $\bar{u}$ is a displacement-like field and $\operatorname{div} F = 0$. A major interest of this decomposition in the present context is that the aforementioned singular behavior of $\bar{\nabla}^S u$ near dislocations is a consequence of its incompatibility, not its divergence. Therefore it can be reasonably assumed that $\nabla^S \bar{u}$ is smooth, as F takes the incompatible part (as $\operatorname{inc} \bar{\nabla}^S u = \operatorname{inc} F$). Joining the Radon-Nikodým and Beltrami decompositions now yields

$$\bar{\nabla}^S u = \nabla^S u + [\![u]\!] \odot N \delta_\Gamma = \nabla^S \bar{u} + F, \tag{3.5}$$

[1]Indeed, without point defects, there are no out-of-plane dislocation movements, hence the displacement field jump is in-plane.

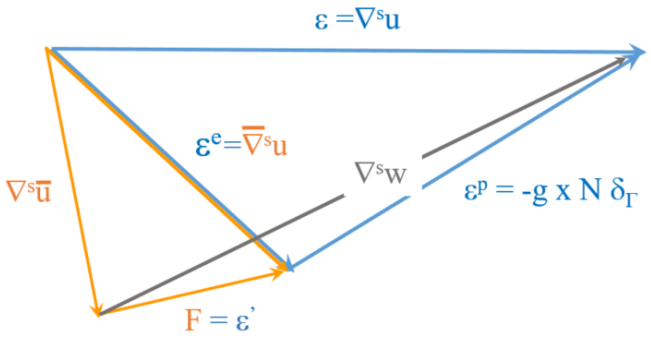

FIGURE 2. Radon-Nikodým (blue) and Beltrami (orange) decompositions.

from which we infer

$$\text{inc } F = \text{ inc } \big([\![u]\!] \odot N\delta_\Gamma\big). \tag{3.6}$$

Additional properties of this construction are given in the following subsections. For illustration purposes we will describe in detail the kinematics of a $2D$ edge dislocation with a glide plane.

3.3. **Mathematical definition of the strain. Main kinematical descriptor.** With the above mathematical background at hand, we are able to accurately define the correction ϵ' in (3.2). We define it as the solution of the minimization problem

$$\min \|\epsilon'\|_{L^2} \qquad \text{such that inc } (\epsilon^e - \epsilon') = 0. \tag{3.7}$$

With the change of unknown $\bar{E} = \epsilon^e - \epsilon'$ this is equivalent to solving

$$\min \|\bar{E} - \bar{\nabla}^S u\|_{L^2} \qquad \text{such that } \text{ inc } \bar{E} = 0.$$

We recognize the orthogonal projection of $\bar{\nabla}^S u$ onto the space of compatible fields. This coincides with the Beltrami decomposition [9, 11] already stated in (3.4):

$$\bar{\nabla}^S u = \bar{E} + F = \nabla^S \bar{u} + F, \qquad \text{div } F = 0.$$

We arrive at

$$\epsilon' = \epsilon^e - \bar{E} = \bar{\nabla}^S u - \nabla^S \bar{u} = F.$$

Finally we obtain using (3.5)

$$E = \epsilon - \epsilon' = \nabla^S u - F = \nabla^S \bar{u} - [\![u]\!] \odot N\delta_\Gamma. \tag{3.8}$$

This will be our main kinematical variable.

3.4. **Decomposition of the displacement.** Let us now define

$$w := u - \bar{u}, \tag{3.9}$$

whereby, using (3.5),

$$\nabla^S w = \nabla^S u - \nabla^S \bar{u} = F - [\![u]\!] \odot N\delta_\Gamma. \tag{3.10}$$

The singular behavior of u is fully contained in w, which means that $\bar{u}$ can be used in the framework of small displacements / small strains. Indeed, the displacement field w, generated intrinsically by the dislocation line, defines an intermediate configuration, upon which the regular displacement $\bar{u}$ is defined. In particular, $\nabla^S \bar{u}$ is considered as small. Schematic representations of all the decompositions at hand are given in Figs. 2 and 3.

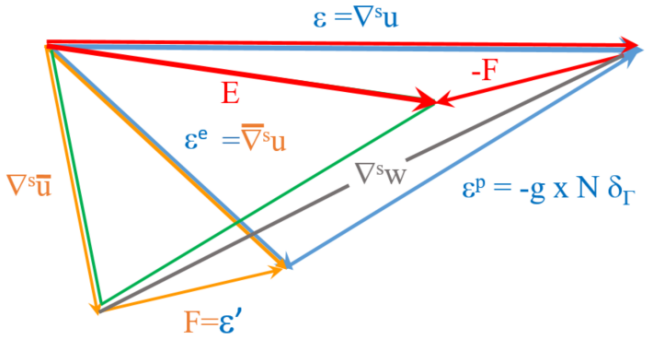

FIGURE 3. The strain of our model satisfies the following decompositions: $E = \nabla^S u - F = \bar{\nabla}^S u - [\![u]\!] \odot N\delta_\Gamma - F = \nabla^S \bar{u} - [\![u]\!] \odot N\delta_\Gamma = \epsilon^e - \epsilon' + \epsilon^p$.

3.5. **Volterra dislocation.** We place ourselves in 2D and assume that the jump $g = [\![u]\!]$ of the displacement field generated by a straight dislocation is prescribed on the glide surface Γ. We are well aware that atomistic representations of "real" dislocations cores with numerical simulations have started in the late 60s [42], and in the 90s for ab initio calculations [13, 41]. Here though, we specifically consider a dislocation line located at the origin and expanding along the z-axis, and a glide half-line Γ, see Fig. 4. In this model g is constant, equal up to a sign to the Burgers vector.

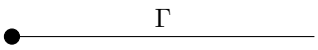

FIGURE 4. Volterra dislocation with glide half-plane

We call Volterra dislocation the kinematics of minimal deformation energy which incorporates the given jump g. It is described by the displacement field w introduced in the preceding subsection. A complete calculation of w in the case of an edge dislocation is developed in Section 4.

$$\min \|\bar{E} - \bar{\nabla}^S u\|_{L^2(C)} \qquad \text{such that } \operatorname{inc} \bar{E} = 0.$$

We recognize the orthogonal projection of $\bar{\nabla}^S u$ onto the space of compatible fields. This coincides with the Beltrami decomposition [9, 11]

4. Closed form for the Volterra edge dislocation

The geometrical setting is as described in Section 3.5 and Fig. 4, but we place ourselves in $\Omega = \mathbb{R}^2$. We specialize to the edge dislocation, with jump

$$g = -be_1 \text{ on } \Gamma. \tag{4.1}$$

Here b is the constant magnitude of the Burgers vector, (e_1, e_2) is the canonical basis of $\mathbb{R}^2$. The Burgers vector itself is be_1.

4.1. **Decomposition of the strain: the incompatible absolutely continuous part.** We have from (3.6)

$$\operatorname{inc} F = \operatorname{inc} (g \odot N\delta_\Gamma).$$

Consider a test tensor field $\Phi = \varphi e_z \otimes e_z$. The expression of the incompatibility in the sense of distributions yields

$$\langle \operatorname{inc} F, \Phi \rangle = \int_\Gamma (g \odot N) \cdot \operatorname{inc} \Phi,$$

from which we infer using (4.1)

$$\langle \operatorname{inc} F, \Phi \rangle = \int_\Gamma b\partial_{12}\varphi = -b\partial_2\varphi(0).$$

We arrive at

$$\operatorname{inc} F = b\partial_2\delta_0 e_3 \otimes e_3 = -\operatorname{Curl} \kappa, \qquad \kappa = b\delta_0 e_3 \otimes e_1.$$

This is consistent with the Kröner formula (3.3) and the construction (3.8). Recall that $\operatorname{div} F = 0$, hence, up to boundary conditions which are here a decay at infinity, F is completely defined by its incompatibility and its divergence. With $\Psi = \psi e_3 \otimes e_3$ we have $\operatorname{inc}\operatorname{inc}\Psi = \Delta^2\psi e_3 \otimes e_3$, whereby $\Delta^2\psi = b\partial_2\delta_0$. An appropriate solution expressed in polar coordinates is $\psi = \frac{br}{8\pi}(2\log r + 1)\sin\theta$. From this we arrive at

$$F = \frac{b}{4\pi r}\begin{pmatrix} \sin\theta(2+\cos 2\theta) & -\cos\theta\cos 2\theta & 0 \\ -\cos\theta\cos 2\theta & -\sin\theta\cos 2\theta & 0 \\ 0 & 0 & 0 \end{pmatrix}.$$

We remark that $|F| \ll 1$ when $r \gg b$. Thus the spatial range of the correction field F is proportional to the Burgers vector magnitude.

4.2. **Dislocation displacement field.** We are now in position to search for one displacement field w satisfying (3.10) with $u = w$. Tedious calculations lead to

$$w = \frac{b}{8\pi}\begin{pmatrix} -4\theta - \sin 2\theta \\ 2\log r + \cos 2\theta \end{pmatrix}. \tag{4.2}$$

The displacement field w is illustrated in Fig. 5. Note that for this kinematics of pure dislocation ($\bar{u} = 0$) we have

$$E = \nabla^S w - F = \nabla^S w - \bar{\nabla}^S w = be_1 \odot e_2\delta_\Gamma, \tag{4.3}$$

which is obviously trace-free.

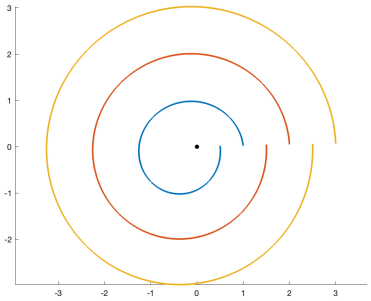

FIGURE 5. Deformation of concentric circles by the Volterra edge dislocation w ($b = 0.5$)

4.3. **Dislocation glide.** We now model the motion of an edge dislocation along its glide plane, by a dislocation dipole. This amounts to placing two Volterra dislocations with opposite Burgers vectors, as displayed in Fig. 6. We observe that the deformation $\nabla^S u$ has a concentrated part on the glide plane and takes significant values nearby dislocation cores. Indeed, in our model according to (4.3), E is concentrated on the glide plane. Furthermore, one observes that the leftmost vertical line, lying at circa $7b$ from the core is almost unaffected by the displacement.

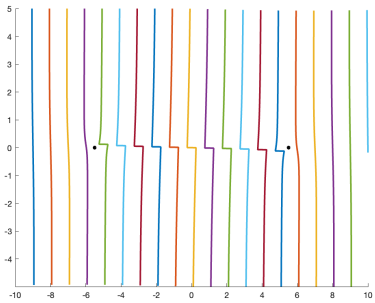

FIGURE 6. Deformation of vertical lines by motion of the Volterra edge dislocation w ($b = 0.5$). The figure illustrates the stock of dislocations after one time step: the dislocation with negative sign means that one dislocation has left its previous location, whereas the positive sign means that a dislocation has reached the new location. Indeed, there is a glide from one pole to the other.

5. Kinematics at the continuum scale

5.1. **Change of scale and macroscopic strain.** We assume that the medium is filled by a distribution of dislocations tending to a continuum. We denote by ε a characteristic ratio related to the magnitude of the Burgers vector of individual dislocations (as divided by the diameter of the crystal), therefore going to 0. We denote by u_ε, E_ε and F_ε the kinematical quantities defined as above. We assume that boundedness properties allow us to have weak limits of form

$$u_\varepsilon \overset{L^2}{\rightharpoonup} u, \qquad E_\varepsilon \overset{\mathcal{M}}{\rightharpoonup} E, \qquad (\varepsilon \to 0),$$

namely in L^2 and in the (weak-$\star$) sense of measure [7], respectively. These assumptions are supported by (3.8) and the general construction provided that the total length of the glide lines scales with ε^{-1}. We further assume that $u \in H^1(\Omega;\mathbb{R}^3)$ and $E \in L^2(\Omega;\mathbb{S}^3)$ (indeed, mathematical analysis of the governing equations at the macroscopic scale allows us to prove this regularity [11]). Setting $F = \nabla^S u - E \in L^2(\Omega;\mathbb{S}^3)$ we infer that $F_\varepsilon \rightharpoonup F$ in the sense of distributions and $\operatorname{div} F = 0$.

5.2. **Macroscopic properties.** Because E is not a priori compatible, the above construction retains some information on the underlying microstructure.

(1) We have seen that F concentrates near dislocation cores, therefore $E \approx \nabla^S u$ at distance from dislocations, where the medium behaves like a classical continuum with compatible slips.
(2) The Beltrami decomposition
$$E = \nabla^S u - F \qquad \text{with } \operatorname{div} F = 0$$
is unique up to appropriate boundary conditions. Therefore E can be chosen as the primary kinematical descriptor, allowing to recover the displacement as a byproduct.
(3) In view of
$$\operatorname{inc} F = -\operatorname{inc} E,$$
the field E encodes the incompatibility characterizing infinitesimal defects, see the discussion of Section 3.

5.3. **Example 1.** Consider a uniform density ρ of edge dislocations with fixed Burgers vector be_1 within the rectangle $Q = [-\frac{h_1}{2}, \frac{h_1}{2}] \times [-\frac{h_2}{2}, \frac{h_2}{2}]$, i.e.,

$$\kappa = \alpha^T = b\,\rho\,\chi_Q\, e_3 \otimes e_1.$$

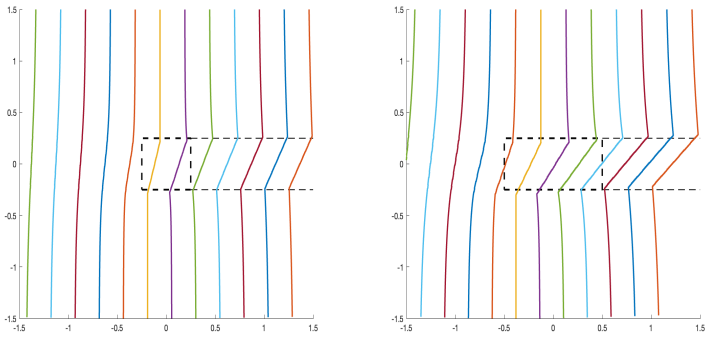

FIGURE 7. Uniform distribution of Volterra dislocations in a square (example 1). Deformation of vertical planes by the displacement field w for $\rho = 1$, $b = 1$, $h_1 = h_2 = 1$ (left), $h_1 = 2, h_2 = 1$ (right). The strain E is a pure shear supported in the horizontal band, with a linear profile in the square becoming constant on the rightmost part.

We compute the corresponding kinematical fields by summation of elementary Volterra dislocations described in Section 4. Mathematically, this is expressed in the form of convolutions as

$$E = \rho E_{\text{meso}} * \chi_Q, \qquad w = \rho w_{\text{meso}} * \chi_Q \tag{5.1}$$

with w_{meso} and E_{meso} given by (4.2) and (4.3), respectively. Using that $\partial_1 E_{\text{meso}} = b\,\delta_0 e_1 \odot e_2$ we obtain $\partial_1 E = \rho \chi_Q e_1 \odot e_2$, from which we infer

$$E = \rho\, b\, f\, e_1 \odot e_2$$

with $f(x) = 0$ if $|x_2| > h_2/2$ or $x_1 < -h_1/2$ (outside the dotted band in Fig. 7), otherwise $f(x) = \min(h_1, x_1 + h_1/2)$. Of course, $\operatorname{tr} E = 0$. The displacement field w is computed numerically from (5.1) and represented in Fig. 7. Here also, the deformation $\nabla^S w$ is accounted by E in the shear band, and approximated in the vicinity of dislocation cores.

5.4. **Example 2.** We assume that

$$\kappa = \alpha^T = \frac{b}{\pi R} \partial_1 \chi_B e_3 \otimes e_1.$$

where B is the ball of center 0 and radius R. Recall that $\nabla \chi_B = -N_B \delta_{\partial B}$, with N_B the outwards unit normal vector to B, hence $\partial_1 \chi_B = -N_B \cdot e_1 \delta_{\partial B}$. This models an horizontal motion of dislocations within B. The chosen scaling allows be_1 to have the dimension of a Burgers vector. Note that there is no glide surface outside B, as opposed to the previous example, because κ has zero mean. In this case we can perform fully analytic calculations.

Similarly to the previous example we compute E by

$$E = \frac{1}{\pi R} \partial_1 \left(\chi_B * E_{\text{meso}} \right) = \frac{1}{\pi R} \chi_B * \partial_1 E_{\text{meso}} = \frac{b}{\pi R} \chi_B e_1 \odot e_2.$$

Here the strain is a constant shear supported in B. Again, the associated stress is trace-free and can be controlled by weakening the shear modulus in this region, see the next section. Then we compute F using $\operatorname{div} F = 0$ and

$$\operatorname{inc} F = -\operatorname{Curl} \kappa = \frac{b}{\pi R} \partial_{12} \chi_B e_3 \otimes e_3.$$

We perform this computation with the help of the decomposition

$$F(x) = \frac{b}{\pi R} \partial_{12} F_1(\frac{x}{R}), \qquad \operatorname{inc} F_1 = \chi_{B_1} e_3 \otimes e_3, \qquad \operatorname{div} F_1 = 0, \tag{5.2}$$

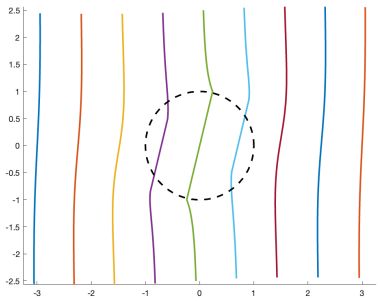

FIGURE 8. Deformation of vertical planes by the displacement field w in example 2. The strain E is constant in B. ($R = 1$, $b = 2$).

with B_1 the unit ball. As in Section 4 we search for $F_1 = \operatorname{inc} \Psi$, $\Psi = \psi e_3 \times e_3$, $\Delta^2 \psi = \chi_{B_1}$. We find $\psi = \frac{1}{64}(r^4 - 1)\chi_{\{r<1\}} + \frac{1}{16}(2r^2 \log r - r^2 + \log r + 1)\chi_{\{r>1\}}$, which yields

$$\partial_{12}\psi = \frac{1}{16} r^2 \sin 2\theta \chi_{\{r<1\}} + \frac{1}{16}(2 - \frac{1}{r^2}) \sin 2\theta \chi_{\{r>1\}}.$$

Using $F(x) = \frac{b}{\pi R} \operatorname{inc} \partial_{12}\Psi(\frac{x}{R})$ we obtain

$$F = -\frac{b}{8\pi R} \begin{pmatrix} 0 & 1 \\ 1 & 0 \end{pmatrix} \qquad \text{in } B.$$

Next we compute F_1 outside B_1 by

$$F_1 = \operatorname{inc} \Psi = \frac{2\log r + 1}{8} \begin{pmatrix} 1 & 0 \\ 0 & 1 \end{pmatrix} + \frac{1}{16}(\frac{1}{r^2} - 2) \begin{pmatrix} \cos 2\theta & \sin 2\theta \\ \sin 2\theta & -\cos 2\theta \end{pmatrix},$$

then

$$\partial_2 F_1 = \frac{1}{4r} \begin{pmatrix} \sin\theta(2 + \cos 2\theta) & -\cos\theta \cos 2\theta \\ -\cos\theta \cos 2\theta & -\sin\theta \cos 2\theta \end{pmatrix} + \frac{1}{8r^3} \begin{pmatrix} -\sin 3\theta & \cos 3\theta \\ \cos 3\theta & \sin 3\theta \end{pmatrix}.$$

We identify that $\partial_2 F_1 = \bar{\nabla}^S w_1$ with

$$w_1 = \frac{1}{8} \begin{pmatrix} -4\theta - \sin 2\theta \\ 2\log r + \cos 2\theta \end{pmatrix} + \frac{1}{16r^2} \begin{pmatrix} \sin 2\theta \\ -\cos 2\theta \end{pmatrix}.$$

In view of (5.2) this leads to $F = \nabla^S v$ outside B with

$$v = \frac{b}{8\pi} \left[\frac{R}{r} \begin{pmatrix} 3\sin\theta + \sin 3\theta \\ 3\cos\theta - \cos 3\theta \end{pmatrix} + \frac{R^3}{r^3} \begin{pmatrix} -\sin 3\theta \\ \cos 3\theta \end{pmatrix} \right].$$

We now compute the displacement field w in order to satisfy the Beltrami decomposition $E = \nabla^S w - F$, which results in

$$\nabla^S w = E + F = \begin{cases} \dfrac{3b}{4\pi R} \chi_B e_1 \odot e_2 \text{ in } B \\ \\ \nabla^S v \text{ outside } B. \end{cases}$$

This is achieved by choosing $w = v$ outside B and the continuous extension

$$w = \frac{3br}{8\pi R} \begin{pmatrix} \sin\theta \\ \cos\theta \end{pmatrix} = \frac{3b}{8\pi R} \begin{pmatrix} x_2 \\ x_1 \end{pmatrix} \qquad \text{in } B.$$

The displacement field w is represented in Fig. 8.

6. Macroscopic linearized mechanical model

6.1. **Cauchy stress.** At this stage we place ourselves in the vicinity of a natural configuration, i.e. a material configuration without residual efforts or deformations (i.e. with vanishing internal stress for vanishing external loading).We insist on the fact that, in this study, only Neumann boundary conditions are treated. In this case, there are no conditions on the kinematic variables at the boundary, and no clamping conditions [15]. We assume that the Cauchy stress satisfies the linear law

$$\Sigma = \mathbb{A}E, \tag{6.1}$$

where $\mathbb{A}$ is an effective elasticity tensor, possibly different from the elastic one. Here, the Cauchy stress corresponds to the classical concept of an internal effort that works against a priori compatible virtual strains. Therefore the internal work expended against a compatible virtual strain $\hat{E}$ is

$$W_{\rm int}(\hat{E}) = \int_\Omega \mathbb{A}E \cdot \hat{E}.$$

The effective tensor $\mathbb{A}$ in (6.1) will be assumed to depend on an internal variable θ, which will be later part of the unknowns. We already see from the example of Subsection 5.3 that $\mathbb{A}$, more specifically the shear modulus, may differ from the elasticity tensor, because the deformation is elasto-plastic, not only where dislocations accumulate but also in regions where glides occur (as in the square and the band in Example 1). Outside these regions we believe reasonable to consider the elastic moduli, because $E \approx \nabla^S u$ at distance of dislocations (related to the decay of F).

6.2. **Governing equations.** The virtual work principle writes in its general form

$$\int_\Omega \mathbb{A}E \cdot \hat{E} = W_{\rm ext}(\hat{E}) = \int_\Omega \mathbb{K} \cdot \hat{E}$$

for every compatible field $\hat{E}$. Here the tensor $\mathbb{K}$ is simply a Riesz representative of the external work $W_{\rm ext}(\hat{E})$. It represents a generalized external force that works against $\hat{E}$. Typically, $W_{\rm ext}(\hat{E})$ is expressed in terms of the virtual displacement $\hat{u}$, itself a byproduct of $\hat{E}$ through the Beltrami decomposition. If $\mathbb{K}$ is chosen such that $-\operatorname{div}\mathbb{K} = f$ in Ω and $\mathbb{K}N = g$ on $\partial\Omega$ then

$$\int_\Omega \mathbb{K} \cdot \hat{E} = \int_\Omega f \cdot \hat{u} + \int_{\partial\Omega} g \cdot \hat{u} \tag{6.2}$$

whenever $\hat{E} = \nabla^S \hat{u}$, thus the classical work of the external forces f and g against the virtual displacement $\hat{u}$ is retrieved (see [10, 11]).

To extend the virtual work principle to arbitrary virtual strains, we need a few mathematical elements available in [8, 11]. Provided Ω is simply connected, we have the L^2-orthogonal decomposition

$$H^{\rm inc}(\Omega;\mathbb{S}^3) = \mathcal{V} \oplus \mathcal{Z}, \tag{6.3}$$

with

$$H^{\rm inc}(\Omega;\mathbb{S}^3) = \{E \in L^2(\Omega;\mathbb{S}^3),\ \operatorname{inc} E \in L^2(\Omega;\mathbb{S}^3)\},$$
$$\mathcal{V} = \{E \in L^2(\Omega;\mathbb{S}^3),\ \operatorname{inc} E = 0\}, \qquad \mathcal{Z} = \{E \in H^{\rm inc}(\Omega;\mathbb{S}^3),\ \operatorname{div} E = 0, EN = 0 \text{ on } \partial\Omega\}.$$

In addition $\|\operatorname{inc} E\|_{L^2}$ defines an equivalent norm on $\mathcal{Z}$, therefore by Riesz representation there exists $\Lambda \in L^2(\Omega;\mathbb{S}^3)$ such that

$$\int_\Omega (\mathbb{K} - \mathbb{A}E) \cdot \hat{E} = \int_\Omega \Lambda \cdot \operatorname{inc} \hat{E} \qquad \forall \hat{E} \in \mathcal{Z}. \tag{6.4}$$

Note that this Λ is not unique. It may be written in the form $\Lambda = \operatorname{inc}\Phi$ with $\Phi \in \mathcal{Z}$, or more generally by a change of inner product, $\Lambda = \mathbb{B}\operatorname{inc}\Phi$ with $\Phi \in \mathcal{Z}$ and $\mathbb{B}$ a uniformly positive definite tensor field in $L^\infty(\Omega,\mathbb{S}^3)$. By the virtual work principle, we already know that

$$\int_\Omega (\mathbb{K} - \mathbb{A}E) \cdot \hat{E} = 0 \qquad \forall \hat{E} \in \mathcal{V}. \tag{6.5}$$

Summing (6.5) and (6.4) yields

$$\int_\Omega \mathbb{A}E\cdot\hat{E}+\Lambda\cdot\operatorname{inc}\hat{E}=\int_\Omega \mathbb{K}\cdot\hat{E}\qquad\forall\hat{E}\in H^{\operatorname{inc}}(\Omega;\mathbb{S}^3).$$

As we have assumed that the unloaded state is natural, we must ensure that $[\mathbb{K}=0\Rightarrow E=0]$ and $W_{\text{ext}}(E)\geq 0$ for any $\mathbb{K}$. Accordingly, choosing $\mathbb{A}$ positive definite guarantees in the compatible case that $\displaystyle\int_\Omega \mathbb{K}\cdot E=\int_\Omega \mathbb{A}E\cdot E\geq 0$. To ensure that the actual work remains nonnegative also in the incompatible case, we choose the constitutive law $\Lambda=\mathbb{D}\operatorname{inc}E$, with $\mathbb{D}$ a positive-definite tensor field. This is also consistent with the mathematical construction of Λ. With these choices, the aforementioned requirements are met. We arrive at

$$\int_\Omega \mathbb{A}E\cdot\hat{E}+\mathbb{D}\operatorname{inc}E\cdot\operatorname{inc}\hat{E}=\int_\Omega \mathbb{K}\cdot\hat{E}\qquad\forall\hat{E}\in H^{\operatorname{inc}}(\Omega;\mathbb{S}^3).\tag{6.6}$$

This formulation was more directly postulated in our previous work [8], where the well-posedness and the interpretation of the natural boundary conditions was also discussed. In particular, under (6.2), choosing $\hat{E}=\nabla^S\hat{u}\in\mathcal{V}$ yields the standard Neumann condition $\mathbb{A}EN=g$ on $\partial\Omega$. Choosing now $\hat{E}\in H^{\operatorname{inc}}(\Omega;\mathbb{S}^3)$ yields the micro-free condition $\mathcal{T}_0(\mathbb{D}\operatorname{inc}E)=\mathcal{T}_1(\mathbb{D}\operatorname{inc}E)=0$ on $\partial\Omega$, with trace operators $\mathcal{T}_0,\mathcal{T}_1$ derived in [9]. Alternatively, Dirichlet type boundary conditions can be represented by imposing $\mathcal{T}_0(E)=\mathcal{T}_1(E)$ on $\partial\Omega$ within the function space, as discussed in [8], but in both cases future work is needed to address numerical treatment as well as mixed conditions.

6.3. **Macroscopic role of F.** Assume that E solves (6.6), that the loading satisfies (6.2) and that the decomposition of E from (6.3) reads $E=\nabla^S u-F$. By plugging $\hat{E}=\nabla^S u-F$ in (6.2) one obtains $\displaystyle\int_\Omega \mathbb{K}\cdot F=0$. We infer

$$\int_\Omega \mathbb{A}(\nabla^S u-F)\cdot\nabla^S u=\int_\Omega \mathbb{K}\cdot\nabla^S u=\int_\Omega \mathbb{K}\cdot E\geq\int_\Omega \mathbb{A}(\nabla^S u-F)\cdot(\nabla^S u-F).\tag{6.7}$$

This yields

$$\int_\Omega \mathbb{A}(\nabla^S u-F)\cdot F\geq 0,\ \text{whereby}\ \int_\Omega \mathbb{A}\nabla^S u\cdot F\geq 0.\tag{6.8}$$

From (6.7) and (6.8) we obtain

$$\int_\Omega \mathbb{A}(\nabla^S u-F)\cdot(\nabla^S u-F)\leq\int_\Omega \mathbb{A}\nabla^S u\cdot\nabla^S u.$$

This means that in some energetic sense, F indeed plays the role of a correction for $\nabla^S u$.

6.4. **Isotropic constitutive laws.** The simplest choice for $\mathbb{D}$ is $\mathbb{D}:=\frac{1}{\theta}\mathbb{I}_4$ (indicewise, $(\mathbb{I}_4)_{ijkl}=\delta_{ik}\delta_{jl}$), where we have introduced an internal variable $\theta>0$. In other words, $\mathbb{D}$ applies to arbitrary symmetric second order tensors X,Y as

$$\mathbb{D}X\cdot Y=\frac{1}{\theta}X\cdot Y.\tag{6.9}$$

We put θ at the denominator so that letting θ go to 0 prevents incompatibility. This is the elastic limit that we have analyzed rigorously in [8]. Therefore we call θ the *compatibility modulus*. For $\mathbb{A}$ we choose the classical isotropic Hooke law

$$\mathbb{A}X\cdot Y=\kappa_0\operatorname{tr}X\operatorname{tr}Y+2\mu(\theta)\operatorname{dev}X\cdot\operatorname{dev}Y,$$

with $\operatorname{dev}X$ the deviatoric par of X, and κ_0 the bulk modulus. As already mentioned, only the shear modulus depends on θ. We assume the decomposition in series of the shear compliance

$$\frac{1}{\mu(\theta)}=\frac{1}{\mu_0}+\frac{1}{\tilde{\mu}(\theta)},\qquad\tilde{\mu}(\theta)=\frac{k}{\theta},\tag{6.10}$$

with μ_0 the elastic shear modulus. This modeling assumption corresponds to summing the elastic compliance with the extra compliance provided by the dislocation mobility. The explicit expression of k will be given in Section 7.2, and reads $k = \frac{\sigma_Y^2}{4}$ with σ_Y the yield stress.

6.5. **The tangent model.** We consider a time interval $[t_l, t_l + T]$ in which the loading rate $\dot{\mathbb{K}}_l$ as well as the tangent tensors $\mathbb{A}$ and $\mathbb{D}$ are assumed constant in time. The configuration at time t_l may contain internal efforts. The main kinematical variable to describe the increment is the strain rate $\dot{E}$. For consistency, the dissipative variable defining $\mathbb{A}$ and $\mathbb{D}$ will be written $\dot{\theta}$, thus constant in the time interval. We will later use the integrated variable θ to represent the dissipative history in incremental schemes with hardening. We call it compatibility modulus rate.

We postulate that (6.6) translates to this setting as

$$\int_\Omega \mathbb{A}(\dot{\theta})\dot{E}(\dot{\theta}) \cdot \hat{E} + \mathbb{D}(\dot{\theta}) \operatorname{inc} \dot{E}(\dot{\theta}) \cdot \operatorname{inc} \hat{E} = \int_\Omega \dot{\mathbb{K}}_l \cdot \hat{E}, \tag{6.11}$$

in which the unknowns are $\dot{E}$ and $\dot{\theta}$. By doing this, we assume that in the incremental model, (6.11) is still valid even when the configuration at time t_l is not neutral. In view of (6.11), $\dot{E}$ is constant in the time interval.

6.6. **Physical interpretation of $\dot{\theta}$.** The quantity $\mathbb{D} \operatorname{inc} E \cdot \operatorname{inc} E$ has the dimension of an energy per unit volume, therefore $\mathbb{D}$ has the dimension of an energy times a length, with unit $[Jm]$. Writing $\mathbb{D}X \cdot Y = \frac{\chi}{\dot{\theta}} X \cdot Y$, and assuming that $\dot{\theta}$ is interpreted as a scalar density of dislocations per unit time, i.e. with unit $[m^{-2}s^{-1}]$ (that is, the number of dislocation segments crossing a unit surface per unit time), then χ is interpreted as a dissipated energy per unit length of dislocation and per unit time, with unit $[Jm^{-1}s^{-1}]$. We have taken for simplicity $\chi = 1$. Note that the actual dissipation is more complex, since the tangent Hooke tensor also contributes to irreversible effects.

7. Dissipation and flow rule for the first increment

7.1. **Variational form.** Here we restrict ourselves to the first increment $[0, T]$, during which the load is taken as $\mathbb{K} = t\dot{\mathbb{K}}_0$. Further increments will be considered in Section 8. The expended external work is

$$W = \int_0^T \int_\Omega \mathbb{K} \cdot \dot{E} = \frac{T^2}{2} \int_\Omega \dot{\mathbb{K}}_0 \cdot \dot{E}. \tag{7.1}$$

We highlight the dependence of all the quantities on $\dot{\theta}$, and write using (6.11) and (6.9)

$$W(\dot{\theta}) = \frac{T^2}{2} \int_\Omega \dot{\mathbb{K}}_0 \cdot \dot{E}(\dot{\theta}) = \frac{T^2}{2} \int_\Omega \kappa \operatorname{tr}^2 \dot{E}(\dot{\theta}) + 2\mu(\dot{\theta}) |\operatorname{dev} \dot{E}(\dot{\theta})|^2 + \frac{1}{\dot{\theta}} |\operatorname{inc} \dot{E}(\dot{\theta})|^2.$$

The virtual work principle (6.11) can be incorporated in variational form to obtain

$$-W(\dot{\theta}) = \min_{\hat{E}} \Big(\frac{T^2}{2} \int_\Omega \kappa \operatorname{tr}^2 \hat{E} + 2\mu(\dot{\theta}) |\operatorname{dev} \hat{E}|^2 + \frac{1}{\dot{\theta}} |\operatorname{inc} \hat{E}|^2 - \int_\Omega \dot{\mathbb{K}}_0 \cdot \hat{E} \Big). \tag{7.2}$$

7.2. **Dissipation and flow rule.** The dissipation is defined as the difference between the actual work and the reversible case $\dot{\theta} = \dot{\theta}_{\min} \approx 0$, i.e.

$$\mathcal{D}(\dot{\theta}) = W(\dot{\theta}) - W(\dot{\theta}_{\min}).$$

Our flow rule is a principle of maximal dissipation. As discussed in [28] it is a convenient modeling technique that incorporates a straightforward sufficient condition for the second principle of thermodynamics. Here we write it in the form : $\dot{\theta}$ minimizes

$$-W(\hat{\theta}) + \Phi(\hat{\theta}) \quad \text{over} \quad \{\hat{\theta} \geq \dot{\theta}_{\min}\},$$

with Φ a dissipation potential. By imposing Φ to be minimal at $\dot{\theta}_{\min}$ we obtain that $W(\dot{\theta}) \geq W(\dot{\theta}_{\min})$, hence $\mathcal{D}(\dot{\theta}) \geq 0$ (see [8]).

In this single increment we intend to model perfect plasticity. To this aim, we use a positively homogeneous potential [8], namely

$$\Phi(\hat\theta) = \int_\Omega \phi(\hat\theta), \quad \phi(\hat\theta) = \gamma_0 \hat\theta,$$

with $\gamma_0 > 0$ a material parameter. Hence, in view of (7.2), the pair $(\dot E, \dot\theta)$ jointly minimizes

$$\frac{T^2}{2}\int_\Omega \kappa \operatorname{tr}^2 \hat E + 2\mu(\hat\theta)|\operatorname{dev}\hat E|^2 + \frac{1}{\hat\theta}|\operatorname{inc}\hat E|^2 - \int_\Omega \dot{\mathbb{K}}_l \cdot \hat E + \gamma_0 \int_\Omega \hat\theta \tag{7.3}$$

under the constraint $\hat\theta \geq \dot\theta_{\min}$. A necessary and sufficient optimality condition for the minimization with respect to $\hat\theta$ is

$$-T^2\mu'(\dot\theta)|\operatorname{dev}\dot E|^2 + \frac{T^2}{2\dot\theta^2}|\operatorname{inc}\dot E|^2 - \gamma_0 \in N(\dot\theta)$$

with the normal cone $N(\dot\theta) = \{0\}$ is $\dot\theta > \dot\theta_{\min}$, $N(\dot\theta_{\min}) = (-\infty, 0]$. Using (6.10) this is equivalent to

$$\frac{1}{2k}|2T\mu(\dot\theta)\operatorname{dev}\dot E|^2 + |\frac{T}{\dot\theta}\operatorname{inc}\dot E|^2 - 2\gamma_0 \in N(\dot\theta). \tag{7.4}$$

It implies in particular for the squared von Mises stress[2].

$$\sigma_M^2 := |2T\mu(\dot\theta)\operatorname{dev}\dot E|^2 \leq 4\gamma_0 k =: \sigma_Y^2.$$

Consider an experiment of uniaxial traction in 1d. In this situation we have $\operatorname{inc} E = 0$, but plastic effects can nevertheless occur. When dissipation occurs, (7.4) exactly yields $\sigma_M^2 = 4\gamma_0 k = \sigma_Y^2$. In addition, only the product $\gamma_0\dot\theta =: \dot\theta_0$ appears in (7.3) due to $\operatorname{inc} E = 0$. Indeed we can write

$$\tilde\mu(\dot\theta) = \frac{\gamma_0 k}{\gamma_0\dot\theta} = \frac{\sigma_Y^2}{4\dot\theta_0} = \tilde\mu_0(\dot\theta_0).$$

Therefore, by changing the variable $\dot\theta$ to $\dot\theta_0$, the knowledge of κ, μ_0 and σ_Y completely fixes the model and permits to retrieve the spirit of classical perfect plasticity. In the classical theory, perfect plasticity is defined in two steps, one given by an elastic deformation (μ_0) followed by a plastic deformation at a fixed critical stress σ_Y. In our model, there is no such decomposition but instead an effective "neither purely elastic nor purely plastic" deformation given by $\mu(\dot\theta)$, see Fig. 9.

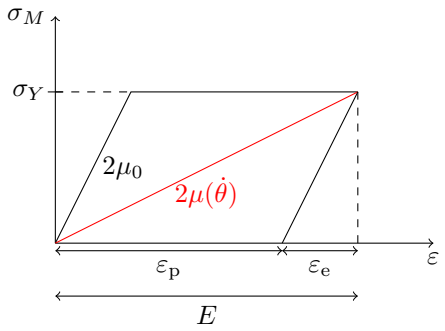

FIGURE 9. Representation of the effective shear modulus on a stress-strain diagram

In order to obtain results of a complete loading-unloading trajectory, the theory obviously needs to be formulated further. We shall then have a curve which, unlike the one shown here, where there is one "big" increment, will be made of several small increments, attaining therefore the plastic

[2]For convenience, our definition of Von Mises stress is made up to a factor $\sqrt{\frac{3}{2}}$.

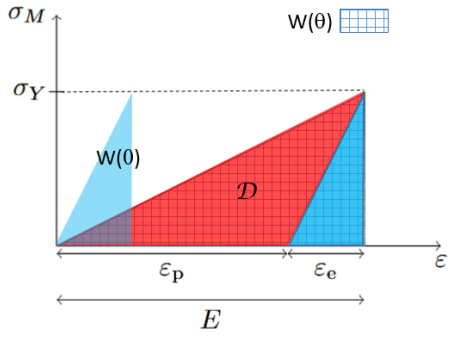

FIGURE 10. Representation of the dissipation as the difference between works

threshold "faster". In the course of implementation, the need to introduce hardening will appear as well.

8. TIME-DISCRETE EVOLUTION SCHEME WITH LOADING AND UNLOADING

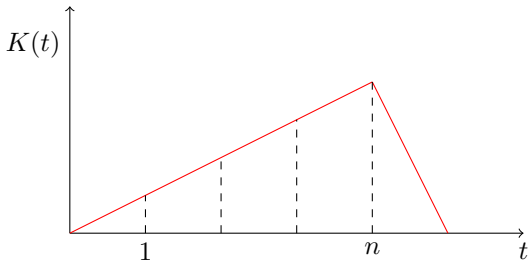

FIGURE 11. Loading-unloading incremental scheme

We now examine a situation where successive increments of load are performed, at times $t_1, \cdots, t_n$, where n is the number of increments - on Fig. 11, the particular case of a constant rate of charge is shown, and $n = 4$. There is then one step of unloading.

8.1. **Incremental setting.** Consider a time increment $[t_l, t_l + T]$ during which the total accumulated loading reads

$$\mathbb{K}(t) = \mathbb{K}_l + (t - t_l)\dot{\mathbb{K}}_l.$$

We further assume that $\dot{\mathbb{K}}_l = \alpha_l \mathbb{Q}$ and $\mathbb{K}_l = \beta_l \mathbb{Q}$. Loading corresponds to $\alpha_l, \beta_l > 0$ and unloading to $\alpha_l < 0, \beta_l > 0$. Let $W_l(\dot{\theta})$ be the expended work during the increment assuming the compatibility modulus rate $\dot{\theta}$. It can be expressed as

$$W_l(\dot{\theta}) = \int_{t_l}^{t_l+T} \int_\Omega \mathbb{K}(t) \cdot \dot{E}_l = \int_\Omega (T\mathbb{K}_l + \frac{T^2}{2}\dot{\mathbb{K}}_l) \cdot \dot{E}_l = (\frac{\beta_l}{\alpha_l}T + \frac{T^2}{2})\alpha_l \int_\Omega \mathbb{Q} \cdot \dot{E}_l. \tag{8.1}$$

Recall that, similarly to (7.2), the virtual work principle yields

$$-\int_\Omega \dot{\mathbb{K}}_l \cdot \dot{E}_l = -\alpha_l \int_\Omega \mathbb{Q} \cdot \dot{E}_l = \min_{\dot{E}} \int_\Omega \kappa_{\mathbb{A}} \operatorname{tr}^2 \dot{E} + 2\mu_{\mathbb{A}}(\dot{\theta}) |\operatorname{dev} \dot{E}|^2 + 2\mu_{\mathbb{D}}(\dot{\theta}) |\operatorname{inc} \dot{E}|^2 - 2\alpha_l \int_\Omega \mathbb{Q} \cdot \dot{E} \tag{8.2}$$

and

$$\alpha_l \int_\Omega \mathbb{Q} \cdot \dot{E}_l = \int_\Omega \kappa_{\mathbb{A}} \operatorname{tr}^2 \dot{E}_l + 2\mu_{\mathbb{A}}(\dot{\theta}) |\operatorname{dev} \dot{E}_l|^2 + 2\mu_{\mathbb{D}}(\dot{\theta}) |\operatorname{inc} \dot{E}_l|^2 \geq 0. \tag{8.3}$$

We distinguish the loading and unloading cases. Beforehand we recall the maximal dissipation principle: the actual compatibility modulus rate $\dot\theta_l \geq \dot\theta_{\min}$ satisfies

$$W_l(\dot\theta_l) - \Phi_l(\dot\theta_l) \geq W_l(\dot\theta) - \Phi_l(\dot\theta) \qquad \forall \dot\theta \geq \dot\theta_{\min}. \tag{8.4}$$

Here Φ_l is a dissipation potential which is minimal at $\dot\theta_{\min}$. This ensures $W_l(\dot\theta_l) \geq W_l(\dot\theta_{\min})$, thus a nonnegative dissipation.

8.2. **Loading.** We have

$$\frac{\beta_l}{\alpha_l}T + \frac{T^2}{2} > 0,$$

therefore (8.1), (8.2) yield $W_l(\dot\theta) \geq 0$. We consider the bilevel minimization problem

$$\min_{\dot\theta\geq\dot\theta_{\min},\dot E} \mathcal{F}_l(\dot E,\dot\theta) := (\frac{\beta_l}{\alpha_l}T + \frac{T^2}{2})\bigg(\int_\Omega \kappa_{\mathbb{A}} \operatorname{tr}^2\dot E + 2\mu_{\mathbb{A}}(\dot\theta)|\operatorname{dev}\dot E|^2 + 2\mu_{\mathbb{D}}(\dot\theta)|\operatorname{inc}\dot E|^2 - 2\alpha_l\int_\Omega \mathbb{Q}\cdot\dot E\bigg) + \Phi_l(\dot\theta).$$

Minimizing w.r.t. $\dot E$ gives $\dot E_l$, solution of the virtual work principle (6.11). This is the desired increment, and the corresponding minimum value is

$$\mathcal{F}_l(\dot E_l,\dot\theta) = -W_l(\dot\theta) + \Phi_l(\dot\theta).$$

Therefore, minimizing $\mathcal{F}_l(\dot E_i,\dot\theta)$ w.r.t. $\dot\theta$ amounts to the desired maximal dissipation principle (8.4). In practice we perform alternating minimizations for $\mathcal{F}_l(\dot E,\dot\theta)$ w.r.t. each variable.

The cumulated strain is computed by

$$\sigma_l = T\sum_{i=0}^{l}\mathbb{A}_i\dot E_i.$$

The corresponding von Mises stress $\sigma_{M,l}$ is computed through the deviatoric part.

8.3. **Elastic unloading.** We will show that the unloading is indeed elastic. When complete unloading is realized in a single increment we have $\mathbb{K}(t_l+T) = \mathbb{K}((n+1)T) = 0$, hence $\alpha_l = -\beta_l/T$. This yields

$$\frac{\beta_l}{\alpha_l}T + \frac{T^2}{2} = -\frac{T^2}{2} < 0.$$

Therefore (8.1), (8.2) yield $W_l(\dot\theta) \leq 0$. Let $\dot E_{\rm el}$ be the elastic solution, corresponding to $\dot\theta = \dot\theta_{\min}$. We have by (8.1), (8.2) for every $\dot\theta \geq \dot\theta_{\min}$,

$$W_l(\dot\theta) \leq -(\frac{\beta_l}{\alpha_l}T + \frac{T^2}{2})\left(\int_\Omega \kappa_{\mathbb{A}}\operatorname{tr}^2\dot E_{\rm el} + 2\mu_{\mathbb{A}}(\dot\theta)|\operatorname{dev}\dot E_{\rm el}|^2 + 2\mu_{\mathbb{D}}(\dot\theta)|\operatorname{inc}\dot E_{\rm el}|^2 - 2\alpha_l\int_\Omega\mathbb{Q}\cdot\dot E_{\rm el}\right).$$

Since $\mu_{\mathbb{A}}$, $\mu_{\mathbb{D}}$ are decreasing functions of $\dot\theta$ we obtain

$$W_l(\dot\theta) \leq -(\frac{\beta_l}{\alpha_l}T+\frac{T^2}{2})\left(\int_\Omega \kappa_{\mathbb{A}}\operatorname{tr}^2\dot E_{\rm el} + 2\mu_{\mathbb{A}}(\dot\theta_{\min})|\operatorname{dev}\dot E_{\rm el}|^2 + 2\mu_{\mathbb{D}}(\dot\theta_{\min})|\operatorname{inc}\dot E_{\rm el}|^2 - 2\alpha_l\int_\Omega\mathbb{Q}\cdot\dot E_{\rm el}\right) = W_l(\dot\theta_{\min}).$$

Thus

$$W_l(\dot\theta) - \Phi(\dot\theta) \leq W_l(\dot\theta_{\min}) - \Phi(\dot\theta_{\min}).$$

The maximal dissipation principle (8.4) yields $\dot\theta_l = \dot\theta_{\min}$ and thus corresponds to a purely elastic unloading, as expected.

A couple of assumptions have been made, as can be noted, during this part of the study:

- first, the parameters $\mathbb{K}_l$ and $\dot{\mathbb{K}}_i$ have been supposed proportional to $\mathbb{Q}$ all throughout, meaning that the nature of the loading remains the same;
- second, we assumed that the unloading is complete.

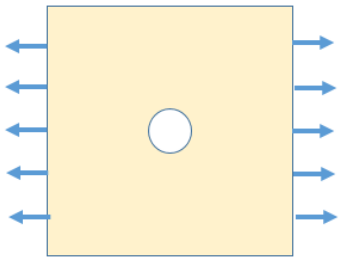

FIGURE 12. Geometry and boundary conditions in the example

9. HARDENING

Perfect plasticity is known to be an unrealistic model, because at the critical stress σ_Y any deformation is allowed without increasing the stress state. On the contrary, laboratory experiments show that at the yield point, the material departs from a pure elastic behavior and becomes ductile, that is, thanks to dislocation movement it is able to deform without breaking. As a matter of fact, the tangent moduli start slowly decreasing, and, tendentially, the strain-stress curve flattens, the rate at which the stress increases is lower than in the elastic domain, slowly decreasing after some threshold. However, during this plastic deformation, the following phenomenon occurs: the dislocation movement produces additional dislocations, the sliding and the entanglement of which possibly hinders the motion. This increases the force needed to move the dislocations and strengthens the metal: it is called *hardening*. In other words, the yield stress (that is, the resistance to failure) increases during plastic deformation, while the material loses its ductility: it becomes harder.

Moreover, beyond the yield stress, if the load is removed, the unloading stress-strain path is different from the loading trajectory, and thus when plastic deformations occur, the stress is actually a history-dependent function of the strain. Indeed, history-dependence is the most characteristic difference between elastic and plastic deformation: as a matter of fact, plastic behaviour does change the material properties, as depending from the loading-unloading history [32] .

In classical models of isotropic hardening based on convex principles, hardening is modeled by increasing the elastic domain, in order to expand the yield surface. This has the required effect of further permitting plastic deformation even if the yield stress has been reached.

In our model, we propose an hardening rule that allows for these requirements:

- makes additional plastic deformation possible after yield;
- takes into account the deformation history;
- allows the material to harden.

Let us now imagine a loading sequence, starting from $\theta = 0$. At some material point, incompatibility occurs and this produces dissipation, therefore $\dot{\theta} > 0$. If an unloading sequence follows, which we assume to be elastic, we have during that time lapse $\dot{\theta} = \dot{\theta}_{\min}$, nevertheless θ retains the history of the loading. We are therefore led to include θ in the expression of the dissipation, taking it to depend on both θ and $\dot{\theta}$. More precisely, we introduce the dissipation potential:

$$\phi_n(\dot{\theta}) := \phi(\theta_n, \dot{\theta}) = \gamma_0 \dot{\theta} \, \exp(-\eta \theta_n) = \gamma_n \dot{\theta},$$

for some material parameter $\eta > 0$, with the accumulated compatibility modulus

$$\theta_n := T \sum_{i=0}^{n-1} \dot{\theta}_i$$

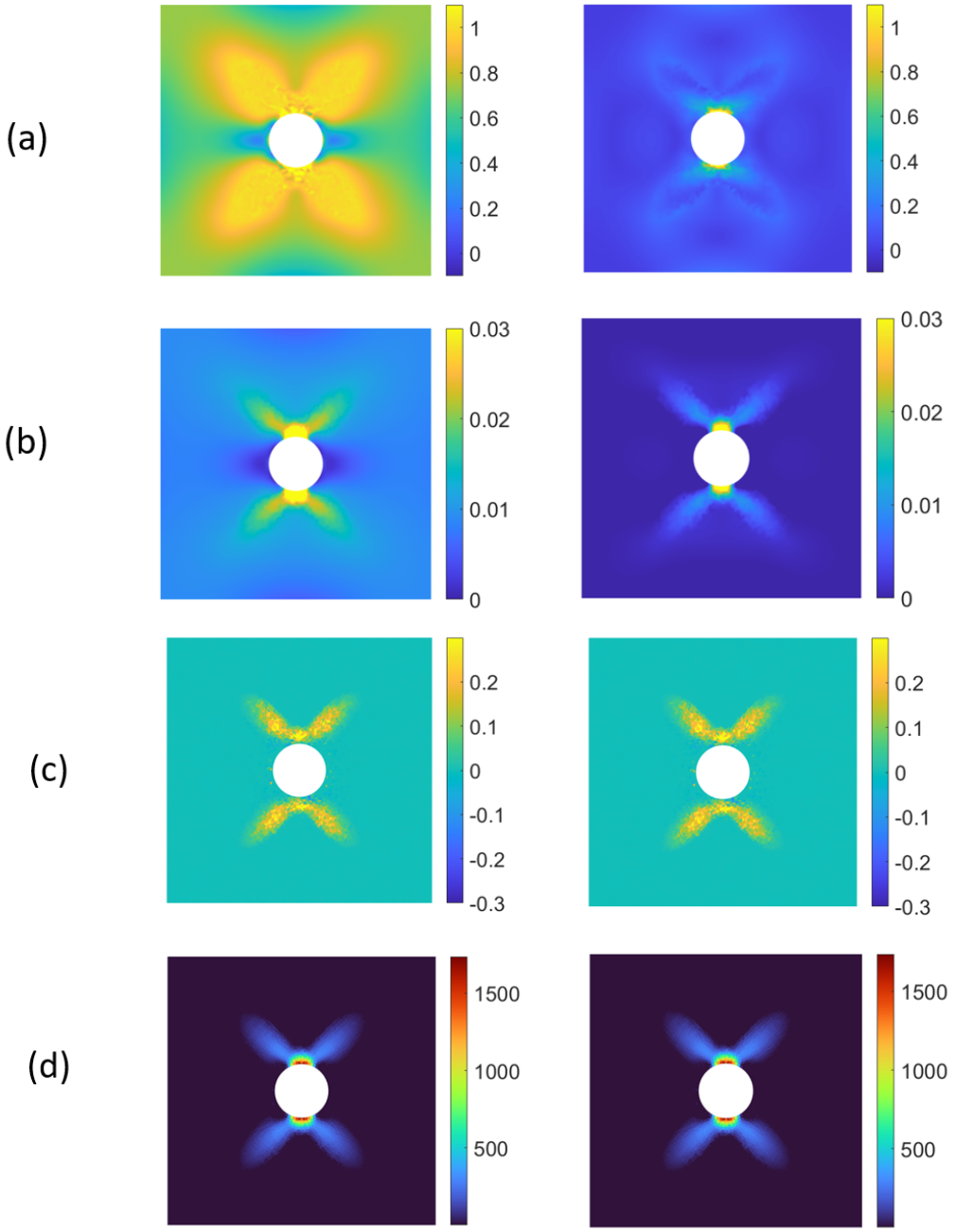

FIGURE 13. First loading, then unloading steps. The (cumulated value) of following quantities are shown: (a) von Mises stress (b) E_{xx}-component of the strain E (c) $(\operatorname{inc} E)_{zz}$ (the only component in $2d$ of the strain incompatibility). (d) compatibility modulus θ (black ≈ 0 for elasticity).

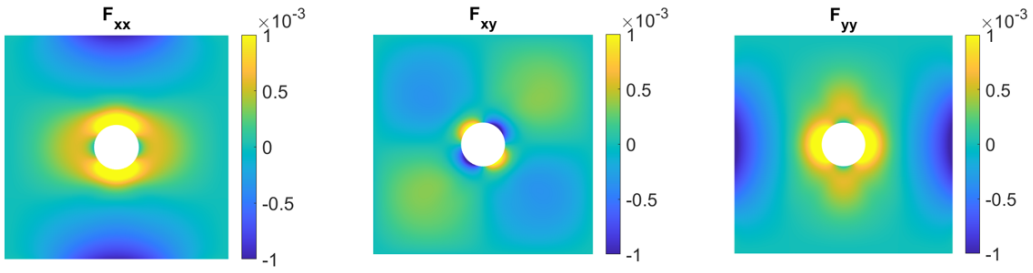

FIGURE 14. Incompatible part F of the strain field E

and where

$$\gamma_0 = \frac{\sigma_Y^2}{4T^2k}, \quad \gamma_n = \gamma_0 \, \exp(-\eta\theta_n) \leq \gamma_0.$$

Note at the first time step starting from an elastic behaviour, $\dot\theta = \dot\theta_{\min}$ and hence $\phi_1(\dot\theta) \approx \phi(\dot\theta) = \gamma_0\dot\theta$. With this at hand, minimality condition with this new potential reads, following (7.4),

$$\frac{1}{2k}|2\mu(\dot\theta)\,\mathrm{dev}E|^2 + |\frac{1}{\dot\theta}\,\mathrm{inc}\;E|^2 = 2\gamma_n. \tag{9.1}$$

Observe that whenever one accumulates plastic strain, one gets $\theta_n > 0$ and increasing, hence γ_n decreasing, thus implying that the tangent moduli decreases while $\dot\theta$ increases, thereby letting both the strain deviatoric part and incompatibility free to evolve according to the mesoscopic dislocation flow, as responsible for both the rise of plastic deformation and hardening effect.

10. Numerical method and numerical simulations

10.1. **Numerical methods.** Equation (7.3) is solved by successive minimizations on $\hat E$ and $\hat\theta$. We refer to [8] where it is shown that the first minimization on $\hat E$ for constant tangent moduli yields $\dot E$ solution of:

$$\int_\Omega \mathbb{A}(\dot\theta)\dot E\cdot\hat E + \mathbb{D}(\dot\theta)\,\mathrm{inc}\;\dot E\cdot\;\mathrm{inc}\;\hat E = \int_\Omega \dot{\mathbb{K}}_1\cdot\hat E \qquad \forall \hat E\in H^{\mathrm{inc}}(\Omega,\mathbb{S}^3). \tag{10.1}$$

It can be solved by looking for a finite element approximation of:

$$\int_\Omega \Big(\mathbb{A}(\dot\theta)(\nabla^S\dot u + \dot E_i)\cdot(\nabla^S\hat u + \hat E_i) + \mathbb{D}(\dot\theta)\,\mathrm{inc}\;\dot E_i\cdot\;\mathrm{inc}\;\hat E_i + \epsilon_u\dot u\cdot\hat u + \nabla^S\dot p\cdot\hat E_i + \dot E_i\cdot\nabla^S\hat p - \epsilon_p\dot p\cdot\hat p\Big)\,dx$$
$$= \int_\Omega f\cdot\hat u dx + \int_{\partial\Omega} g\cdot\hat u dS(x) \qquad \forall(\hat u,\hat E_i,\hat p)\in H^1(\Omega,\mathbb{R}^3)\times H^{\mathrm{inc}}(\Omega,\mathbb{S}^3)\times H^1(\Omega,\mathbb{R}^3), \tag{10.2}$$

where $\nabla^S\dot u + \dot E_i = \dot E = \nabla^S\dot u - \dot F$, f, g are the external body and boundary forces, see (6.2), and ϵ_u, ϵ_p are small positive stabilization parameters. Within FreeFem++, we use HCT elements for $\dot E_i$ and P_2 elements for $\dot u$ and $\dot p$.

The independent variable $\dot\theta$ is then found by dual Newton iterations (Appendix 1 [8]).

10.2. **Numerical simulations.** The first numerical experiment is shown on Fig. 13 and pictures the result of a loading-unloading test. We consider a perforated cylinder in plane stress as represented in Fig. 12. The transverse section is such that there is a disk-shaped hole in the center, we then apply a horizontal load. Obviously, inside the hole, the stress is vanishing, and we expect it to jump to nonzero values on the hole boundary due to loading on the external boundary. In the first increment, we increase the load by a certain amount, and in the second we decrease it of the same magnitude, in order to recover the initial state (zero load). On the first plot, Fig. 13

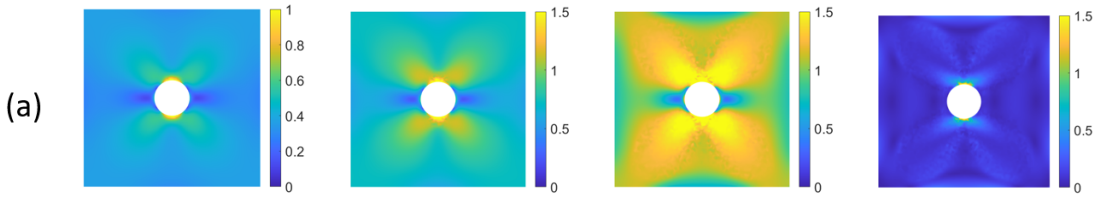

FIGURE 15. Incremental loading steps, then unloading. The von Mises stress for the 1st, 2nd, 3rd and unloading increments is shown.

(a), we observe the von Mises stress: it concentrates on diagonal bands developing from the hole poles towards the boundary of the solid square. The emission of dislocations from the hole poles is likely explained by considering the von Mises map: indeed the nucleation at the surface, where the mobility threshold for dislocations is lower and the stress is high, favors a high dislocation density gradient at these points. On the right plot we observe, as expected in plastic flows, some residual stress after unloading has completed. On the second plot, (b), the xx-component of the strain is shown: it concentrates along the same patterns. On the third, (c), the strain incompatibility is plotted. We recall that Kröner's formula relates this quantity with the rotational of the dislocation density. Since no changes are observed regarding this quantity between the loading and the unloading steps, we deduce that the dislocations did not move between these time steps. This is corroborated by Figure (a), and indeed the residual stresses correspond to the location of the dislocations. Finally, in (d) we have plotted the compatibility modulus, the internal variable introduced to take into account the dissipation phenomena: as expected dissipation initiates at the pole at the highest intensity and develops along the bands, which we can interpret as the glide surfaces of the flow.

The second experiment is depicted in Figures 15 and 16. It consists of a 6-loading increments sequence. On (a) the Von Mises stress is plotted: we see that it is strictly increasing along some diagonal bands starting from the poles. On (b) the xx-stress component is shown: it corresponds to the major traction effects, and therefore is similar to Von Mises. On (c) we have plotted the lower-magnitude xy-stress component. On Figure (d) we have plotted the zz-incompatibility component, and, by Kröner's formula, we may interpret it in terms of dislocation density. For a contortion of form $\kappa = \varphi e_z \otimes b$ with a scalar density φ and a fixed Burgers vector b, we have $\operatorname{Curl} \kappa = -\partial_n \varphi e_z \otimes e_z$, where n is orthogonal to b. Therefore, if φ is some diffuse Dirac mass along a line of direction b then $\operatorname{Curl} \kappa$ admits a negative peak and a positive peak following the direction orthogonal to b. This is clearly visible in the rightmost two plots of Figure (d), where the lines under consideration are the diagonals.

Numerical simulations parameters

Elastic modulus: κ_0; effective shear moduli: μ_A and μ_D; μ_0 elastic shear modulus; σ_Y yield stress; η hardening coefficient; g traction force.

$$\frac{1}{\mu(\dot\theta)} = \frac{1}{\mu_0} + \frac{1}{\tilde\mu}, \text{ where } \tilde\mu(\dot\theta) = \frac{k}{\dot\theta} \text{ and } \mu_D = \frac{1}{2\dot\theta}.$$

g	k	σ_Y	μ_0	κ_0	η
0.5	10^4	1	38.46	83.0	2.10^{-3}

10.3. **Interpretation in terms of dislocation mobility.**

It is elementary yet instructive to look at the maps of the eigenvectors associated with the greatest eigenvalue of the stress tensor, in order to predict the direction of Burgers vector on each

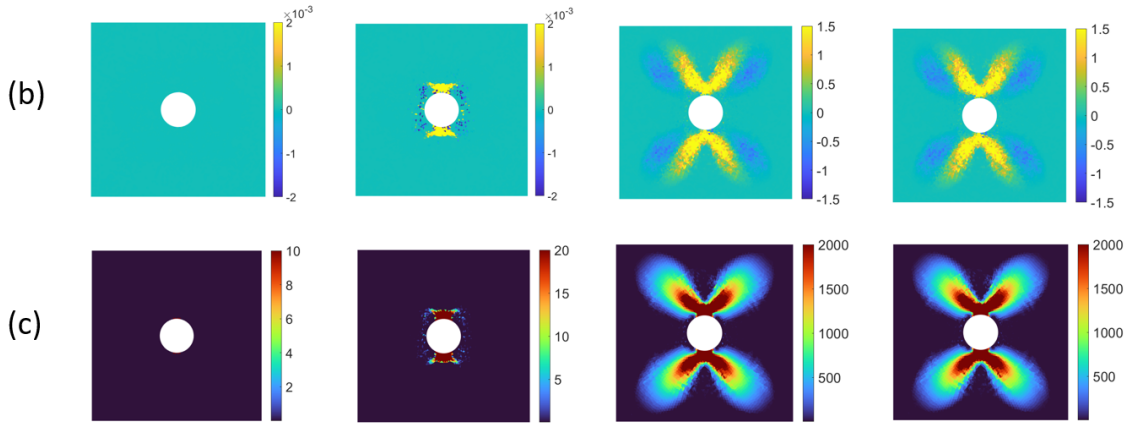

FIGURE 16. Same 3 incremental loading steps and unloading. The following (cumulated) quantities for the 1st, 2nd, 3rd and unloading increments are shown: (b) inc E_{zz}: notice the positive (in yellow) and negative (in blue) value of the field; (c) compatibility modulus θ.

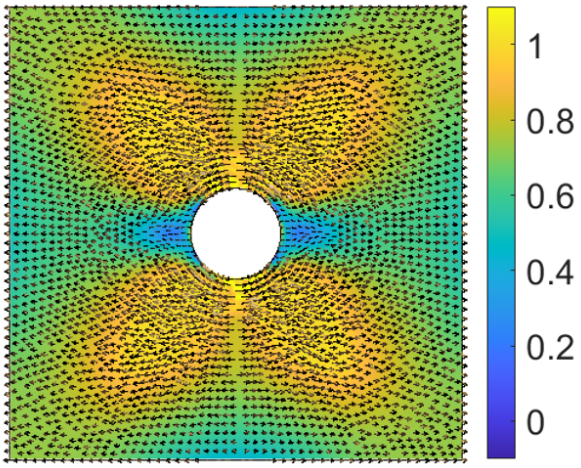

FIGURE 17. Eigenvectors and color map corresponding to the maximum principal stress, which is in-plane except in the dark blue area, where the maximum principal stress is normal to the plane. One increment computation - see Fig 11. (scale factor is arbitrary)

dislocation segment which is submitted to the maximum Peach-Koehler force. The corresponding diagonalization results are shown on Figure 17. As a reminder, in the setting of Figure 18, where b is the Burgers vector, t the unitary vector tangent to the edge dislocation line, n is the unitary normal to b in the section plane, the Peach-Koehler force PK is given by $\mathrm{PK} := (\Sigma.b) \times t$. We call (e_b, e_n, e_t) the basis associated to the dislocation. We restrict ourselves to the main area, outside the dark blue area, where the minimum principal stress is along z and null. In that case PK is in the plane of the section and:

$$\mathrm{PK} = -b\ (\Sigma_{bb} e_n + \Sigma_{bn} e_b)$$

We consider the top right quadrant. θ is the angle of the maximum principal stress with the natural (i, j) basis associated with the coordinates (x, y). If α is the angle between the (e_b, e_n) basis and

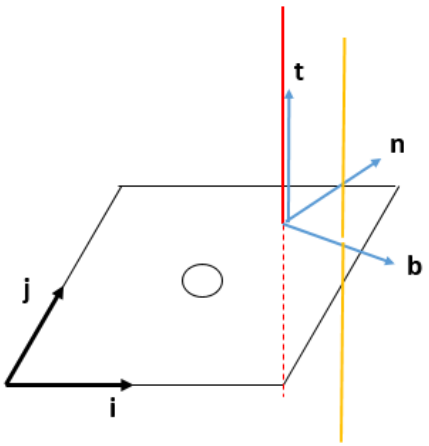

FIGURE 18. Edge dislocation moves from red to yellow under the action of Peach-Koehler force

(i, j) (Figure 18), then it is easy to see that

$$\Sigma_{bb} = \frac{1}{2}(\sigma_1 + \sigma_2) + \frac{1}{2}(\sigma_2 - \sigma_1)\sin(2(\theta - \alpha)$$

$$\Sigma_{bn} = \frac{1}{2}(\sigma_2 - \sigma_1)\sin(2(\theta - \alpha),$$

where $\sigma_{1,2}$ are the eigenvalues of the stress tensor. As an example, if $\theta = 0$, the norm of PK is given by

$$|PK| = \sqrt{(\frac{1}{2}(\sigma_1^2 + \sigma_2^2) + \frac{1}{2}(\sigma_1^2 - \sigma_2^2)\cos(2\alpha)}$$

Discrete dislocation dynamics simulations might give more precise insight into the behaviour of a population of 2D edge dislocations fed by dislocation sources located at the poles, where the stress is at its highest and the nucleation conditions are favorable, and submitted to our computed stress field. In order to perform relevant simulations, attention has to be paid to both boundary conditions and inclusion of our stress field in the calculations. Ideally, the DDD code should be coupled with finite elements, which may be one of the next steps among our numerical benchmarks.

11. CONCLUSION

In this paper the concept of incompatibility has been developed for a modeling purpose, linking the chosen kinematic quantities with the dislocation density tensor, according to the vision of Kröner. Following this, a new definition of the deformation field has been proposed at the meso scale, while its macroscopic counterpart is one the unknowns of the PDE system. This field is given mathematical and physical interpretations by means of the Radon-Nikodým and Beltrami decompositions at the mesoscopic scale. The subsequent decomposition of the displacement $u = w + \bar{u}$ has been illustrated by an analytical calculation in the particular case of a model Volterra dislocation. Construction schemes are given to summarize the successive operations which have led to the definition of the various fields. They show the correspondence between our kinematic description and decompositions, and the traditional ones.

We then presented the macroscopic mechanical model, the bases of which have been set up in the works of Amstutz and Van Goethem [8, 11]. It consists in a time-discrete incremental scheme and

essentially rests on the principle of virtual work and the Clausius-Duhem inequality, the satisfaction of which is obtained by the introduction of an internal variable, called compatibility modulus θ, and its associated rate $\dot{\theta}$, together with a dissipation potential.
The incremental framework has then been worked out for accumulated loadings. The introduction of hardening has been made through a new formula for the dissipation, which takes the history of material deformation into account. This formula differentiates our model from the conventional ones, and remains to be experimentally validated.
The numerical method for this variational and coupled model is based on mixed finite elements, and has been recalled. A series of computations are then given on simple examples to assess our model. First a loading-unloading simulation in two increments has been performed. Results are as expected, and we mention in addition that the elastic unloading behaviour is predicted by our theory. Incremental computations show typical behaviour of the field inc E. More involved numerics is on the way, together with comparisons with computations with conventional models.
An important feature of higher-gradient models is the so-called size-effect issue, i.e., how certain geometric ratios, and sample size, play a role on the onset and propagation of plastic fronts. The assessment of this phenomena within our model, that possesses an internal lengthscale (through $\dot{\theta}$) might be the object of future works. Notice that, physically, plasticity occurs when a *sufficient* amount of dislocations are put into motion, and this requires the existence of a *sufficient* number of dislocation sources. Thus, smaller samples are less likely to deform plastically, and might rather fail at some critical stress. We expect to obtain some results on this feature with our model.
We also would like to investigate the phenomenon of *polygonization*. It consists of specific lower-energy states of microscopic structures due to atomic rearrangements of dislocations. Indeed, in many cases, one can perceive macroscopically constantly curved lattice planes that appear to be microscopically polygonized [26].

Acknowledgments: NVG is supported by FCT - Fundação para a Ciência e a Tecnologia, I.P., through national funds, under the project UID/04561/2025.

References

[1] M. Abatour and S. Forest. Strain gradient plasticity based on saturating variables. European Journal of Mechanics-A/Solids, 104:105016, 2024.
[2] A. Acharya. A model of crystal plasticity based on the theory of continuously distributed dislocations. J. Mech. Phys. Solids, 49(4):761–784, 2001.
[3] A. Acharya, R. J. Knops, and J. Sivaloganathan. On the structure of linear dislocation field theory. J. Mech. Phys. Solids, 130:216–244, 2019.
[4] Amit Acharya. Constitutive analysis of finite deformation field dislocation mechanics. Journal of the Mechanics and Physics of Solids, 52(2):301–316, 2004.
[5] G. Allaire, F. Jouve, and N. Van Goethem. Damage and fracture evolution in brittle materials by shape optimization methods. J. Comput. Physics, 33(16):5010–5044, 2011.
[6] L. Ambrosio, A. Coscia, and G. Dal Maso. Fine properties of functions with bounded deformation. Archive for Rational Mechanics and Analysis, 139(3):201–238, 1997.
[7] L. Ambrosio, N. Fusco, and D. Pallara. Functions of bounded variation and free discontinuity problems. Oxford Mathematical Monographs. Oxford, 2000.
[8] S. Amstutz and N. Van Goethem. A second-order model of small-strain incompatible elasticity. Mathematics and Mechanics of Solids, 29(3):503–530, 2024.
[9] S. Amstutz and N. Van Goethem. Analysis of the incompatibility operator and application in intrinsic elasticity with dislocations. SIAM J. Math. Anal., 48(1):320–348, 2016.
[10] S. Amstutz and N. Van Goethem. Incompatibility-governed elasto-plasticity for continua with dislocations. Proc. R. Soc. A, 473(2199), 2017.
[11] S. Amstutz and N. Van Goethem. Existence and asymptotic results for an intrinsic model of small-strain incompatible elasticity. Discrete Contin. Dyn. Syst., Ser. B, 25(10):3769–3805, 2020.
[12] M. Biot. Thermoelasticity and irreversible thermodynamics. J. Appl. Phys, 27:240, 1956.
[13] Woodward C. and Rao S.I. Ab initio simulation of isolated screw dislocations in bcc mo and ta. Philosophical Magazine A, 71(4):719–735, 1995.
[14] K. S. Cheong and E. P. Busso. Discrete dislocation density modelling of single phase fcc polycrystal aggregates. Acta materialia, 52(19):5665–5675, 2004.

[15] P.G. Ciarlet. Mathematical Elasticity, Vol. I: Three-Dimensional Elasticity. . North-Holland, 1988.
[16] L. De Luca, R. Scala, and N. van Goethem. A new approach to topological singularities via a weak notion of Jacobian for functions of bounded variation. Indiana Univ. Math. J., 73(2):723–779, 2024.
[17] K. S. Djaka, V. Taupin, S. Berbenni, and C. Fressengeas. A numerical spectral approach to solve the dislocation density transport equation. Modelling and Simulation in Materials Science and Engineering, 23(6):065008, 2015.
[18] C. Fressengeas, V. Taupin, and L. Capolungo. An elasto-plastic theory of dislocation and disclination fields. International Journal of Solids and Structures, 48(25-26):3499–3509, 2011.
[19] C. Goodbrake, A. Goriely, and A. Yavari. The mathematical foundations of anelasticity: existence of smooth global intermediate configurations. Proceedings of the Royal Society A, 477(2245):20200462, 2021.
[20] I. Groma, F. Csikor, and M. Zaiser. Spatial correlations and higher-order gradient terms in a continuum description of dislocation dynamics. Acta Mater., 51:1271–1281, 2003.
[21] M. E. Gurtin, E. Fried, and L. Anand. The mechanics and thermodynamics of continua. Cambridge University Press, Cambridge, 2010.
[22] B. Halphen and Q.S. Nguyen. Sur les matériaux standard généralisés. Journal de Mécanique, 14(1):39–63, 1975.
[23] W. Han and B. D. Reddy. Plasticity: mathematical theory and numerical analysis(Vol. 9). . Springer Science and Business Media, 2012.
[24] T. Hochrainer, S. Sandfeld, M. Zaiser, and P. Gumbsch. Continuum dislocation dynamics: towards a physical theory of crystal plasticity. Journal of the Mechanics and Physics of Solids, 63:167–178, 2014.
[25] E. Kröner. Kontinuumstheorie der Versetzungen und Eigenspannungen. Ergebnisse der Angewandten Mathematik. 5. Berlin-Göttingen-Heidelberg: Springer-Verlag. vii, 179 S., 39 Abb. (1958)., 1958.
[26] E. Kröner. Allgemeine kontinuumstheorie der versetzungen und eigenspannungen. Arch. Rat. Mech. Anal., 4:273–334, 1960.
[27] E. Kröner. Continuum theory of defects. Physics of Defects, Les Houches, 35:217–315, 1981.
[28] J. Lemaitre and J.-L. Chaboche. Mechanics of solid materials. Transl. from the French by B. Shrivastava. Foreword to the French edition by Paul Germain, foreword to the English edition by Fred Leckie. Cambridge etc.: Cambridge University Press, 1990.
[29] G. D. Lima-Chaves and M. V. Upadhyay. Finite element implementation of the thermal field dislocation mechanics model: Study of temperature evolution due to dislocation activity. Computer Methods in Applied Mechanics and Engineering, 421:116763, 2024.
[30] S. Lucarini, M. V. Upadhyay, and J. Segurado. Fft based approaches in micromechanics: fundamentals, methods and applications. Modelling and Simulation in Materials Science and Engineering, 30(2):023002, 2021.
[31] G. Maggiani, R. Scala, and N. Van Goethem. A compatible-incompatible decomposition of symmetric tensors in L^p with application to elasticity. Math. Meth. Appl. Sci, 38(18):5217–5230, 2015.
[32] L. E. Malvern. Introduction to the Mechanics of a Continuous Medium. Prentice-Hall series in engineering of the physical sciences. Prentice-Hall, 1969.
[33] T. Mura. Micromechanics of defects in solids. . Springer Science and Business Media, 2013.
[34] R. Scala and N. Van Goethem. Geometric and analytic properties of dislocation singularities. P Roy Soc Edimb A, 2018.
[35] R. Scala and N. Van Goethem. A variational approach to single crystals with dislocations. SIAM J. Math. Anal., 51(1):489–531, 2019.
[36] J. C. Simo and T. J. R. Hughes. Computational inelasticity. Springer, Berlin, 1998.
[37] K. Starkey, G. Winther, and A. El-Azab. Theoretical development of continuum dislocation dynamics for finite-deformation crystal plasticity at the mesoscale. Journal of the Mechanics and Physics of Solids, 139:103926, 2020.
[38] N. Van Goethem. Strain incompatibility in single crystals: Kröner's formula revisited. J. Elast., 103(1):95–111, 2011.
[39] N. Van Goethem and F. Dupret. A distributional approach to $2D$ Volterra dislocations at the continuum scale. Europ. Jnl. Appl. Math., 23(3):417–439, 2012.
[40] N. Van Goethem and F. Dupret. A distributional approach to the geometry of $2D$ dislocations at the continuum scale. Ann. Univ. Ferrara, 58(2):407–434, 2012.
[41] Clouet E. Ventelon L., Willaime F and Rodney D. Ab initio investigation of the peierls potential of scrw dislocations in bcc iron. Acta Materialia, 59(11):4934–4947, 2011.
[42] V. Vitek. Intrinsic stacking faults in body-centred cubic crystals. Philosophical Magazine, 18:773–786, 1968.
[43] G. Z. Voyiadjis and M. Yaghoobi. Size Effects in Plasticity: From Macro to Nano. Elsevier Science, 2019.
[44] M. Xavier, N. Van Goethem, and A. A. Novotny. A simplified model of fracking based on the topological derivative concept. International Journal of Solids and Structures, 139-140:211 – 223, 2018.
[45] A. Yavari and A. Goriely. Riemann–Cartan geometry of nonlinear dislocation mechanics. Archive for Rational Mechanics and Analysis, 205(1):59–118, Jul 2012.
[46] H. Ziegler. An attempt to generalize onsager's principle, and its significance for rheological problems. Zeitschrift für angewandte Mathematik und Physik, 9b:748–763, 1958.

Appendix to 7.2

We comment here on the generality and structure of the equation (7.3), which has been demonstrated and discussed in detail in preceding work [8]. In isothermal quasi-static conditions, the general form of the Rayleigh-Onsager relation yields [22, 46]:

$$(\dot{\mathbf{u}}, \dot{\boldsymbol{\theta}}) = \underset{(\dot{\mathbf{u}}', \dot{\boldsymbol{\theta}}')}{\operatorname{Arg\,min}} \int_\Omega \left[\dot{\Psi}(\mathbf{u}', \boldsymbol{\theta}') + \dot{\Phi}(\dot{\boldsymbol{\theta}}') - \mathbf{f} \cdot \dot{\mathbf{u}}' \right] dV$$

where Ψ is the free energy and Φ the dissipation. The term with $\dot{\Psi} + \dot{\Phi}$ is minimized (corresponding to maximization of the dissipation) under the condition of equilibrium of the external and internal powers (term in $\mathbf{f} \cdot \dot{\mathbf{u}}'$).
Ψ should be determined so as to obey Biot's coupling equation, which sets an interdependence between the free energy and the dissipation, namely [12, 22]:

$$-\frac{\partial \Psi}{\partial \boldsymbol{\theta}} + \frac{\partial \Phi}{\partial \dot{\boldsymbol{\theta}}} = 0$$

The left term is null, signifying there is no direct action of an external force on the internal variable in the case of plasticity. This equation has been addressed in [8], leading to the linear expression of $\Phi(\theta)$ found in (7.3).
With these two components the determination of the problem is complete.

Laboratoire de Mathématiques d'Avignon, Avignon Université, 301 rue Baruch de Spinoza, 84916 Avignon Cedex
Email address: samuel.amstutz@univ-avignon.fr

Solid Mechanics Laboratory (LMS), CNRS, Ecole Polytechnique, Institut Polytechnique de Paris, 91128 -Palaiseau Cedex
Email address: thien-nga.le@polytechnique.edu

Universidade de Lisboa, Faculdade de Ciências, Departamento de Matemática, CEMS.UL, Alameda da Universidade, C6, 1749-016 Lisboa, Portugal
Email address: vangoeth@fc.ul.pt